

# Aberrant adenosine A<sub>2A</sub> receptor signaling in the choroid plexus drives CSF hypersecretion and ventriculomegaly in hydrocephalus

Received: 24 February 2025

Accepted: 14 November 2025

Published online: 07 December 2025

 Check for updates

Wu Zheng<sup>1,2,8</sup>  , Lanxin Hu<sup>1,3,8</sup>, Yuwen Yang<sup>1,3,8</sup>, Xuhang Li<sup>1</sup>, Jia Wu<sup>4</sup>, Wangchao Chen<sup>1</sup>, Yiwei Jiang<sup>1</sup>, Yuhan Chen<sup>1</sup>, Hongcai Wang<sup>5</sup>, Shiwei Li<sup>5</sup>, Kuan Feng<sup>5</sup>, Cheng Zheng<sup>1</sup>, Yanjiang Wang<sup>6</sup>, Rodrigo A. Cunha<sup>7</sup>, Zhongyue Lv<sup>2</sup>   & Jiang-Fan Chen<sup>1,3</sup>  

Hydrocephalus is a common and serious neuropathological condition characterized by disrupted cerebrospinal fluid (CSF) circulation, which lacks effective pharmacotherapy. Here, we demonstrate that adenosine A<sub>2A</sub> receptor (A<sub>2A</sub>R) signaling in the choroid plexus (ChP) is a trigger of hydrocephalus. Adenosine levels are increased in the CSF of hydrocephalus patients and mice, together with elevated ChP-A<sub>2A</sub>R density. Accordingly, continued infusion of adenosine for 14 days or transgenic ChP-A<sub>2A</sub>R overexpression is sufficient to drive CSF hypersecretion and ventriculomegaly. Conversely, selective knock-down of ChP-A<sub>2A</sub>R reduces CSF production and ameliorates CSF hypersecretion and ventriculomegaly induced by autologous blood and kaolin. Furthermore, we unveil ChP-A<sub>2A</sub>R signaling as a molecular mechanism linking brain insults with CSF hypersecretion through parallel PI3K/Akt-dependent activation of SPAK phosphorylation and NF-κB-dependent transcriptional regulation of ATP1A2. Lastly, the A<sub>2A</sub>R antagonist KW6002 protects against hydrocephalus induced by autologous blood and kaolin, offering a novel treatment for hydrocephalus by repurposing the FDA-approved A<sub>2A</sub>R antagonist istradefylline.

Hydrocephalus is a common and serious neurological condition characterized by the enlargement of the cerebrospinal fluid (CSF)-filled ventricles in the brain, impairing brain development in children and causing neurodegeneration in adults<sup>1</sup>. Although hydrocephalus is a potentially devastating condition, effective prevention strategies are lacking, and shunt revision surgery remains the

mainstay of treatment (accounting for nearly one third of all neurosurgical procedures in the United States), despite frequent complications and high mortality<sup>1</sup>. The efforts to develop alternative pharmacotherapies for hydrocephalus patients have largely failed due to an incomplete understanding of the pathogenesis of hydrocephalus.

<sup>1</sup>The Eye-Brain Research Center and Molecular Neuropharmacological Lab, State Key Laboratory of Ophthalmology, Optometry and Visual Science, Eye Hospital, Wenzhou Medical University, Wenzhou, Zhejiang, China. <sup>2</sup>Department of Neurology, the Affiliated Lihuili Hospital, Ningbo University, Ningbo, Zhejiang, China. <sup>3</sup>Oujiang Laboratory (Zhejiang Laboratory for Regenerative Medicine, Vision and Brain Health), School of Ophthalmology & Optometry and Eye Hospital, Wenzhou Medical University, Wenzhou, Zhejiang, China. <sup>4</sup>Key Laboratory for Laboratory Medicine, Ministry of Education, Zhejiang Provincial Key Laboratory of Medical Genetics, School of Laboratory Medicine and Life Science, Wenzhou Medical University, Wenzhou, Zhejiang, China. <sup>5</sup>Department of Neurosurgery, Ningbo Medical Center Lihuili Hospital, Ningbo University, Ningbo, Zhejiang, China. <sup>6</sup>The Department of Neurology, Daping Hospital, The Arm Medical University, Chongqing, China. <sup>7</sup>CNC-Center for Neuroscience and Cell Biology, Faculty of Medicine, University of Coimbra, Coimbra, Portugal. <sup>8</sup>These authors contributed equally: Wu Zheng, Lanxin Hu, Yuwen Yang.  e-mail: [zheng123wu@163.com](mailto:zheng123wu@163.com); [lzy\\_neuro@163.com](mailto:lzy_neuro@163.com); [chenjf555@gmail.com](mailto:chenjf555@gmail.com)

The enlargement of CSF-filled ventricles is traditionally attributed to a decreased CSF reabsorption and an impediment in CSF outflow, although CSF hypersecretion by the choroid plexus (ChP) in response to infection, hemorrhage or traumatic insult, is increasingly recognized to play a role in the onset and progression of hydrocephalus<sup>2,3</sup>. In particular, in the development of post-infectious (PIH) and post-hemorrhagic hydrocephalus (PHH), ChP triggers CSF hypersecretion in response to infection, hemorrhage, and traumatic insults. This secretory response may be initially adaptive to maintain homeostasis by clearing pathogenic organisms or debris, but becomes maladaptive eventually promoting ventriculomegaly and elevated intracranial pressure<sup>4</sup>. Accordingly, hypersecretion of CSF resulting from ChP hyperplasia or tumors is sufficient to cause non-obstructive hydrocephalus<sup>5</sup>. Several ChP-enriched epithelial transport proteins critically controlling CSF production were identified by genetic and pharmacological studies, including sodium-coupled bicarbonate transporters, AQP1 water-channels<sup>6</sup> and particularly Na<sup>+</sup>/K<sup>+</sup>/2Cl<sup>-</sup> cotransporters (NKCC1), which contribute to approximately half of the production of CSF<sup>7</sup>. And recent studies show that the targeted inhibition of SPAK (STE20/SPS1-related proline/alanine-rich kinase)-NKCC1 in the ChP alleviates kaolin-induced hydrocephalus, post-infectious and PHH<sup>4,8,9</sup>.

While the ChP-enriched epithelial transport proteins controlling CSF production have been identified, the molecular link coupling brain infection and hemorrhage (trauma) with CSF hypersecretion and development of hydrocephalus is unknown. We now hypothesize that the ChP-adenosine-A<sub>2A</sub>R signaling may serve as a molecular link between inflammation/infection/trauma and CSF hypersecretion. Adenosine is increasingly recognized as an important signal mediating adaptive stressful response, such as upon trauma, infection or inflammation<sup>10</sup>, which are the main triggers of ChP-mediated CSF hypersecretion in hydrocephalus. Accordingly, adenosine levels are markedly increased during transient forebrain ischemia and subsequent reperfusion<sup>11,12</sup>, traumatic brain injury<sup>13</sup> and brain infection<sup>14</sup>. Adenosine exerts its effects by activating G-protein coupled receptors, with a prominent role of A<sub>2A</sub>R in the control of brain dysfunction<sup>15</sup>. Accordingly, we recently demonstrated that A<sub>2A</sub>R expression in the ChP is induced in an experimental autoimmune encephalomyelitis model<sup>16</sup> and the selective knockdown of A<sub>2A</sub>R in the ChP prevents T-cell infiltration into the brain and mitigates immunologically-induced brain injury<sup>16,17</sup>. Furthermore, we have also previously reported that astrocytic A<sub>2A</sub>R are physically associated and control the activity of Na<sup>+</sup>-K<sup>+</sup>-ATPases<sup>18</sup>, which are a determinant of transmembrane fluxes in ChP epithelial cells<sup>19</sup>. This raises the exciting possibility that the aberrant adenosine-A<sub>2A</sub>R signaling in ChP may serve as a molecular link between inflammation/infection/trauma with CSF hypersecretion via A<sub>2A</sub>R-Na<sup>+</sup>-K<sup>+</sup>-ATPase interaction, which would prompt ChP-A<sub>2A</sub>R as a potentially new target for the pharmacological treatment of hydrocephalus.

In this study, we demonstrated an aberrantly increased CSF-adenosine and ChP-A<sub>2A</sub>R signaling in hydrocephalus mouse models and patients. The selective overexpression or knockdown of A<sub>2A</sub>R and ATP1A2 in ChP, coupled with pharmacological treatment with A<sub>2A</sub>R antagonists, uncovered ChP-A<sub>2A</sub>R signaling as a molecular mechanism linking brain inflammation with CSF hypersecretion and ventriculomegaly via the SPAK/ATP1A2 cascade. This prompts a novel strategy for treating hydrocephalus with high translational potential by targeting the aberrant ChP-A<sub>2A</sub>R signaling with the FDA-approved A<sub>2A</sub>R antagonist KW6002.

## Results

### Adenosine signaling is aberrantly elevated in the CSF and ChP in hydrocephalus

To explore potential changes of adenosine levels within the CSF in the context of hydrocephalus pathology, we collected CSF samples from patients with different clinically defined conditions of hydrocephalus

(*n* = 11) and age-matched controls with different neurological conditions without hydrocephalus (*n* = 8) (Table S1). HPLC analysis revealed that the median adenosine concentration in the CSF of controls was 0.242 μM (interquartile range: 0.029–0.337), and it was significantly elevated in the CSF of hydrocephalus patients, showing approximately a five-fold increase, with a median level of 1.038 μM (interquartile range: 0.673–3.204) (Fig. 1A–C).

Given that the ChP is surrounded by self-secreted CSF, we hypothesized that these increased CSF levels of adenosine might contribute to hydrocephalus pathology by activating adenosine receptors located in the ChP. Among adenosine receptors, A<sub>2A</sub>R plays a crucial role in the control of inflammation<sup>20</sup> and brain trauma<sup>15</sup>, as well as in transmembrane transport<sup>21</sup>. Therefore, we resorted to a PHH model in mice through intracerebroventricular (ICV), based on injection of autologous blood, to investigate putative alterations of A<sub>2A</sub>R. Five days after administration of autologous blood, MRI analysis revealed that PHH mice had larger ventricles compared to mice treated with PBS (Fig. 1D, E). In parallel, PHH mice also displayed increased CSF levels of adenosine (Fig. 1F) and a significant increase of A<sub>2A</sub>R immunofluorescent staining in the ChP (Fig. 1G, H). To identify the cell types where A<sub>2A</sub>R was upregulated in PHH mice, we observed that the increased A<sub>2A</sub>R signals did not co-localize with IBA-1 (macrophages/microglia), CD31 (endothelial cells) or MHC-II (antigen-presenting cells, APCs) and were superimposed with intercellular cell adhesion molecule-1 (ICAM-1, ChP epithelium) staining (Fig. 1I, J). Similarly, we induced obstructive hydrocephalus in mice by ICV injection of kaolin (Fig. S1A, B) and found increased adenosine levels in CSF and elevated A<sub>2A</sub>R signals in the ChP at 10 days after the injection (Fig. S1C–G). These findings collectively suggest that aberrant adenosine/A<sub>2A</sub>R signaling in both the CSF and ChP is present and may play a role in the pathology of hydrocephalus.

### ChP-specific overexpression of A<sub>2A</sub>Rs increases CSF secretion and triggers hydrocephalus

To ascertain the role of A<sub>2A</sub>R signaling, we induced A<sub>2A</sub>R overexpression in the ChP of wild-type (WT) mice by ICV injection of AAV2/5-CMV-A<sub>2A</sub>R-HA (A<sub>2A</sub>R-OE) or AAV2/5-CMV-EGFP viruses (Fig. 2A). After two weeks, through observation of EGFP and HA staining, we confirmed that the overexpression of A<sub>2A</sub>R was restricted to the ChP tissue and co-localized perfectly with the HA-tag (Fig. 2B, C). Additionally, no HA signal, which reported the presence of the injected AAV2/5-CMV-A<sub>2A</sub>R-HA, was observed in other brain regions (Figs. S2 and S3). Western blot analysis of ChP lysates further confirmed that ICV injection of AAV2/5-CMV-A<sub>2A</sub>R-HA increased A<sub>2A</sub>R protein levels (Fig. 2D, E).

Two weeks after ICV-injection of the viruses, MRI scans were conducted to quantify the size of the brain ventricles. Figure 2F, G shows that A<sub>2A</sub>R overexpression selectively in the ChP resulted in enlarged brain ventricles without altering brain volume (Fig. 2H). Ex vivo DAPI staining of brain sections further confirmed the increased ventricular size induced by A<sub>2A</sub>R overexpression (Fig. 2I, J). Accordingly, the measurement of CSF content demonstrated a significant increase in CSF secretion (Fig. 2K, L).

We next examined the status of CSF outflow in A<sub>2A</sub>R-OE mice by administering the CSF tracer Evans Blue into the lateral ventricles of both A<sub>2A</sub>R-OE and control mice. Our observations revealed unimpeded distribution of the dye through the cerebral aqueduct and all ventricles, indicating the presence of aqueduct patency and the maintenance of bulk CSF flow (Fig. 2M)<sup>3</sup>.

These findings provide robust support for the assertion that overexpression of A<sub>2A</sub>R in the ChP enhances CSF secretion and leads to an increase in ventricular size.

### ChP-specific knockdown of A<sub>2A</sub>Rs decreases CSF secretion and ventricular size

To further investigate the role of aberrant A<sub>2A</sub>Rs signaling in the ChP, we conducted a ChP-selective knockdown of A<sub>2A</sub>R (A<sub>2A</sub>R-Kd) through

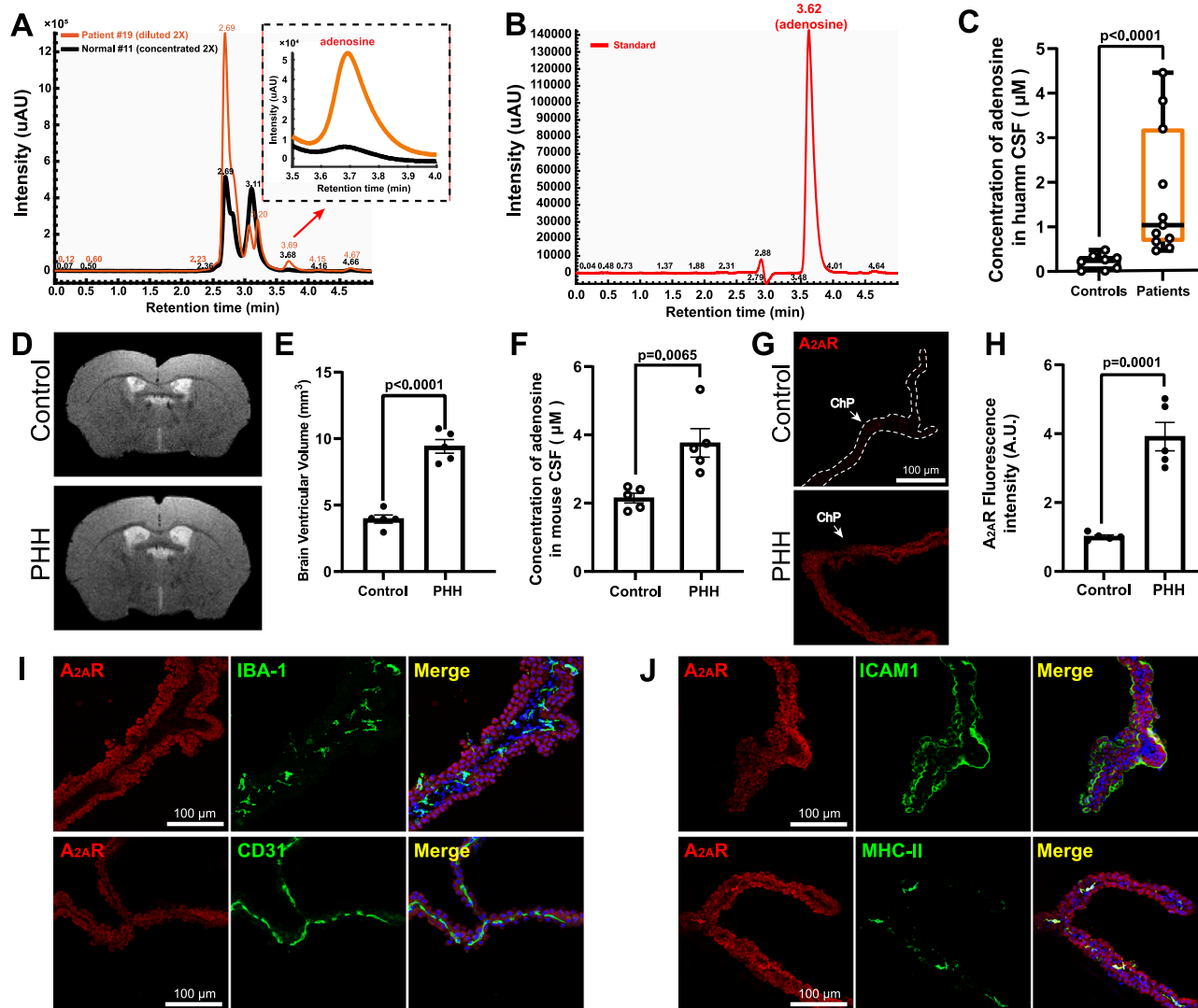


**Fig. 1 | Aberrant adenosine signaling during hydrocephalus in the cerebrospinal fluid (CSF) and choroid plexus (ChP).** **A** Representative chromatogram depicting adenosine levels in the CSF of both control subjects and hydrocephalus patients. **B** Chromatogram illustrating the adenosine standard (5  $\mu\text{mol/L}$ ). **C** Average adenosine concentrations in the CSF of control subjects ( $n = 8$ ) and hydrocephalus patients ( $n = 11$ ). The box plots show the centre line (median), the bounds of the box (25th and 75th percentiles), and the whiskers (minima and maxima). **D** Representative fMRI images capturing brain ventricles dimensions on day 5 post-ICV injection of PBS (control) or autologous blood (PHH) into WT mice ( $n = 5$ /group). **E** Quantification of brain ventricles sizes as shown in **(D)** ( $n = 5$ /group).

**F** Adenosine concentration in the CSF of mice 5 days after ICV-injection with PBS (control) or autologous blood ( $n = 5$ /group). **G** Images of  $A_{2A}R$  immunostaining in the ChP of mice 5 days after ICV-injection with PBS (control) or autologous blood ( $n = 5$ /group). **H** Quantitative analysis of  $A_{2A}R$  fluorescence intensity as illustrated in **(G)** ( $n = 5$ /group). **I, J** The lack of co-staining of  $A_{2A}R$  with different cell markers (IBA-1 for microglia, CD31 for endothelial cells, MHC-II for lymphocytes) contrasts with the co-localization with ICAM-1 (a marker of ChP epithelium) in the ChP of mice 5 days after ICV-injection with autologous blood ( $n = 5$ /group). Unpaired two-tailed Student's  $t$  test, except in **(C)** (Two-tailed Mann-Whitney U test). Data are mean  $\pm$  s.e.m. Source data are provided as a Source Data file.

ICV-injection in WT mice of AAV2/5 carrying a shRNA targeting *adora2a* or a scramble control (AAV2/5-U6-shRNA( $A_{2A}R$ )-Kd-CMV-EGFP or AAV2/5-U6-scramble-CMV-EGFP). Two weeks post-injection, we employed MRI to assess potential changes in ventricular size (Fig. 3A). To validate the ChP-specific  $A_{2A}R$  knockdown with our method, we tracked the fluorescence distribution of the injected AAV2/5 labeled with EGFP. EGFP signals were exclusively located in the ChP in both scramble and  $A_{2A}R$ -Kd groups (Fig. 3B). A qPCR analysis showed that the AAV2/5 carrying the shRNA targeting  $A_{2A}R$ , achieved a near 80% knockdown efficiency (Fig. 3C). To systematically assess the EGFP distribution, we also screened its potential expression in major organs and tissues (heart, liver, spleen, lung, kidney, dura mater and cervical lymph node). However, no EGFP signals were detected (Fig. S4). Strikingly, the specific knockdown of  $A_{2A}R$  in the ChP led to an almost complete loss of the ventricles

(Fig. 3D, E), whereas total brain volume remained unchanged (Fig. 3F). This was confirmed with DAPI staining of brain sections, which also revealed a significant reduction in ventricular size upon  $A_{2A}R$  knockdown (Fig. 3G, H). When we measured the CSF content by collecting CSF from the cisterna magna during 15 min, we found that virtually no CSF could be extracted from the  $A_{2A}R$ -Kd mice (Fig. 3I, J).

### Genetic deletion of $A_{2A}R$ s in the ChP and pharmacological inhibition of the $A_{2A}R$ s mitigate hydrocephalus induced by autologous blood and kaolin

Our findings strongly suggest that  $A_{2A}R$  signaling in the ChP plays a pivotal role in CSF secretion. Therefore, we hypothesized that deactivating  $A_{2A}R$  signaling could mitigate ventriculomegaly in hydrocephalus. Initially, we suppressed the expression of  $A_{2A}R$  in the ChP

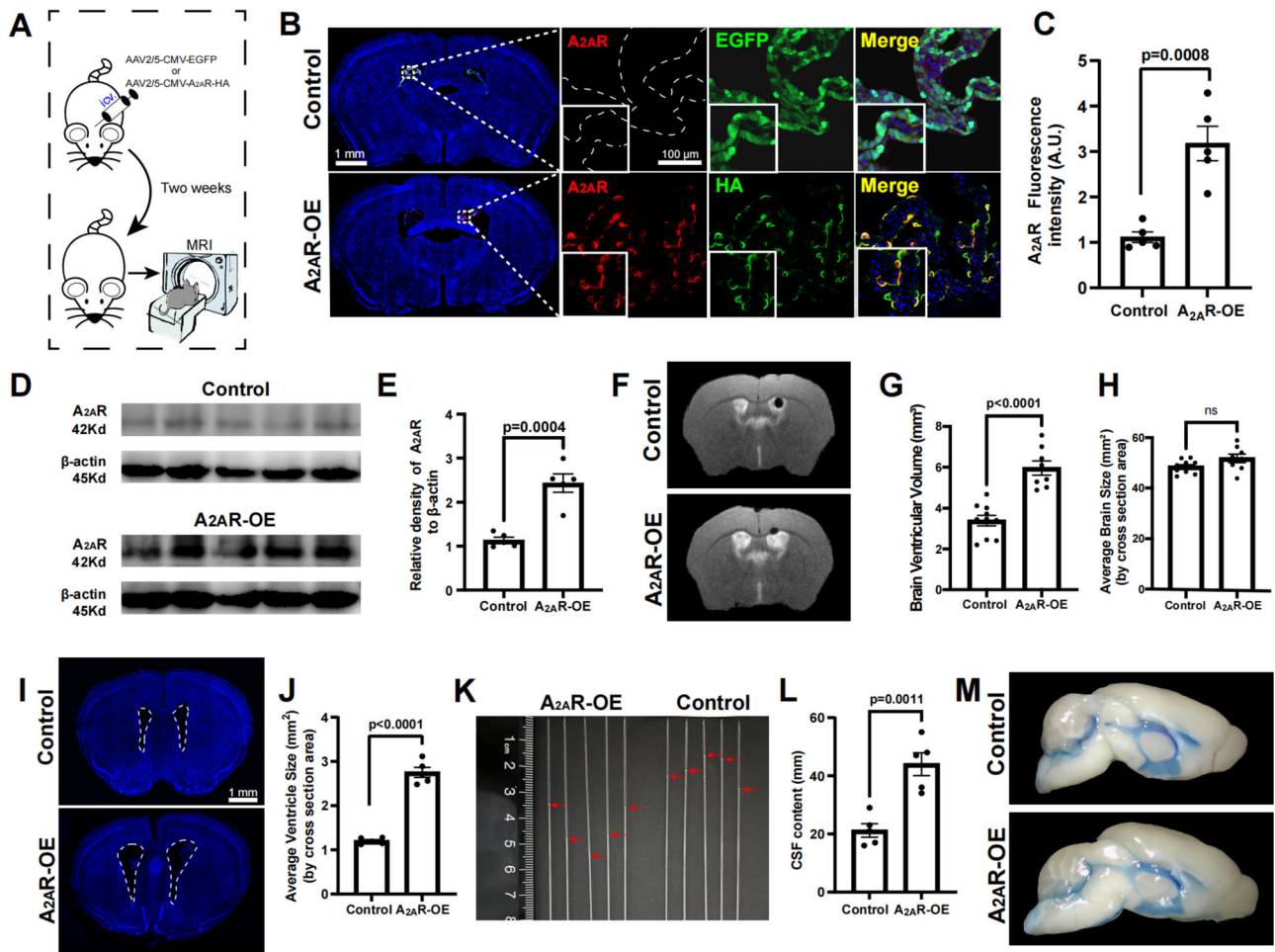


**Fig. 2 | Overexpression of A<sub>2A</sub>R selectively in the choroid plexus (ChP) (A<sub>2A</sub>R-OE) leads to cerebrospinal fluid (CSF) hypersecretion and enlarged ventricles.**

**A** Scheme of the experimental design for exploring the impact of A<sub>2A</sub>R overexpression in the ChP using fMRI. **B** Representative immunofluorescence images of HA-tag (labeling A<sub>2A</sub>R) or EGFP in brain sections transduced with AAV2/5-A<sub>2A</sub>R-OE or control virus on day 14 following ICV viral injection. **C** Quantitative analysis of A<sub>2A</sub>R fluorescence intensity as shown in **(B)** ( $n = 5$ /group). **D** Representative immunoblots comparing ChP lysates from AAV-control vs. AAV-A<sub>2A</sub>R-OE mice (14 days after ICV-viral injection). **E** Quantification of A<sub>2A</sub>R protein levels from the Western blots illustrated in **(D)** ( $n = 5$ /group). **F** Representative fMRI images showing brain ventricles, obtained

14 days after induction of A<sub>2A</sub>R overexpression in the ChP. **G** Ventricular volumes of mice in control vs. A<sub>2A</sub>R-OE mice (control  $n = 10$ , A<sub>2A</sub>R-OE  $n = 8$ ). **H** Brain sizes of mice in control vs. A<sub>2A</sub>R-OE mice (control  $n = 10$ , A<sub>2A</sub>R-OE  $n = 8$ ). **I** Representative DAPI-stained images showing lateral ventricles after 14 days of ChP-targeted A<sub>2A</sub>R overexpression ( $n = 5$ /group). **J** Quantitative analysis of ventricular size as shown in **(I)** ( $n = 5$ /group). **K** Representative measurement of the CSF content of mice in the control vs. A<sub>2A</sub>R-OE group. **L** Quantitative analysis of CSF content as shown in **(K)** ( $n = 5$ /group). **M** Representative of flow trajectories of Evans blue dye (injected into the lateral ventricles) in control and A<sub>2A</sub>R-OE mice. Unpaired two-tailed Student's *t* test. ns: non-significant. Data are mean  $\pm$  s.e.m. Source data are provided as a Source Data file.

through ICV injection of AAV2/5-U6-shRNA (A<sub>2A</sub>R)-Kd-CMV-EGFP virus in WT mice. After a two-week interval, we induced PHH model in the mice. After 5 days, we evaluated lateral ventricle volumes by MRI (Fig. 4A). A<sub>2A</sub>R staining showed that the A<sub>2A</sub>R-Kd virus effectively reduced the protein abundance of A<sub>2A</sub>R in the ChP (Fig. 4B, C). The MRI data unequivocally showed that mice with A<sub>2A</sub>R knockdown exhibited reduced ventriculomegaly, as compared to control mice (Fig. 4D). Specifically, the average volume of the ventricles in A<sub>2A</sub>R-Kd mice was less than one-third of that observed in the hydrocephalus mice treated with mock virus (Fig. 4E). In addition, no discernable alterations of brain volume were noted (Fig. 4F).

In our previous studies, we have established that the intraperitoneal injection (i.p.) of the A<sub>2A</sub>R selective antagonist, KW6002, can exert a pharmacological effect on the ChP<sup>16,22</sup>. Consequently, following the ICV injection of autologous blood into WT mice, the mice received a daily i.p. treatment with KW6002 (5 mg/kg) (Fig. 4G). After 5 days, MRI analysis revealed that KW6002 was effective in alleviating the autologous blood-induced ventricle enlargement (Fig. 4H, I) without altering brain volume (Fig. 4J).

Moreover, we also performed obstructive hydrocephalus induced with kaolin. The data showed that inactivation of A<sub>2A</sub>R in ChP by genetic (Fig. SSA–F) or pharmacological (Fig. SSG–J) method also improved obstructive hydrocephalus. We detect the expression of other adenosine receptors (A<sub>1</sub>, A<sub>2B</sub>, A<sub>3</sub>) in hydrocephalus (kaolin-induced and PHH). As the data showed, there were no obvious changes in those receptors (Fig. S6). These results strongly imply that the targeted modulation of the aberrant A<sub>2A</sub>R signaling in the ChP ameliorates the morphological hallmark of hydrocephalus. This prompts the possibility that inactivating A<sub>2A</sub>R specifically in the ChP could hold a therapeutic promise for hydrocephalus.

#### Aberrant A<sub>2A</sub>R signaling in the ChP regulates CSF secretion by triggering a PI3K-dependent phosphorylation of SPAK

SPAK serves as a regulatory scaffold within a multi-ion transporter complex, located in the ChP epithelium, that critically regulates CSF production<sup>4</sup>. In the context of the post-infectious hydrocephalus, the active form of SPAK (p-SPAK) is upregulated within the ChP, and the

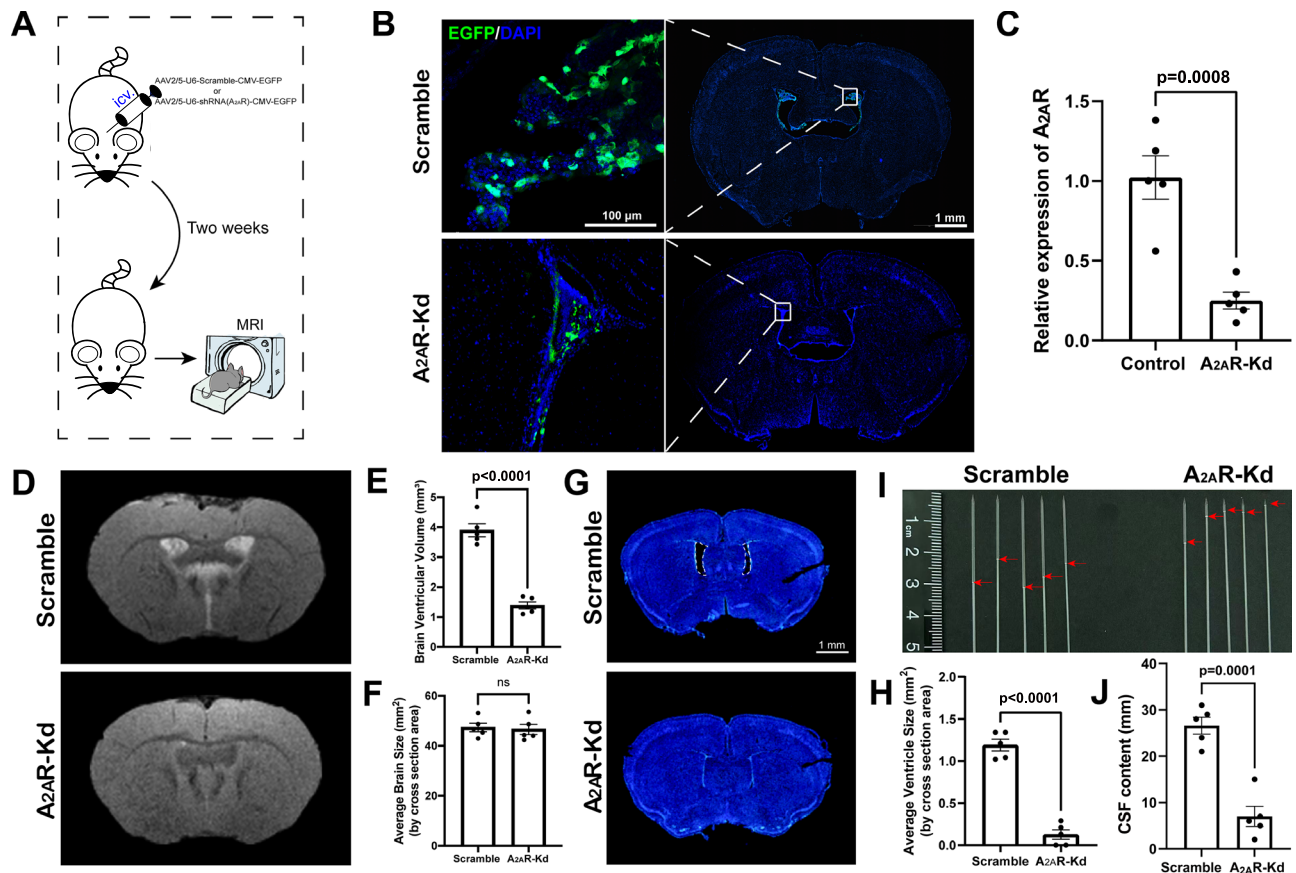


**Fig. 3 | Choroid plexus (ChP)-selective knockdown of  $A_{2A}R$  ( $A_{2A}R$ -Kd) leads to reduced cerebrospinal fluid (CSF) secretion and ventricular size.** **A** Scheme of the experimental design to investigate the impact of  $A_{2A}R$  knockdown in the ChP using fMRI. **B** Representative immunofluorescence images showing EGFP staining in the brain (right) and in particular in the ChP (left) of mice 14 days after ICV-injection with scramble (control) virus or virus expressing shRNA to down-regulate  $A_{2A}R$  ( $A_{2A}R$ -Kd) ( $n = 5$ /group). **C** qPCR analysis showed that the mRNA level of  $A_{2A}R$  was reduced by  $A_{2A}R$ -Kd virus ( $n = 5$ /group). **D** Representative fMRI images showing the size of brain ventricles 14 days after  $A_{2A}R$  knockdown in the ChP. **E** Ventricle

volumes of mice in the scramble vs.  $A_{2A}R$ -Kd group ( $n = 5$ /group). **F** Brain sizes of mice in the scramble vs. the  $A_{2A}R$ -Kd group ( $n = 5$ /group). **G** Representative DAPI-stained images depicting lateral ventricles 14 days after  $A_{2A}R$  knockdown. **H** Quantification of ventricular size as shown in (**G**) ( $n = 5$ /group). **I** Representative measurement of the CSF content of mice in the scramble vs.  $A_{2A}R$ -Kd group. **J** Quantitative analysis of CSF content in (**I**) ( $n = 5$ /group). Unpaired two-tailed Student's *t* test. ns: non-significant. Data are mean  $\pm$  s.e.m. Source data are provided as a Source Data file.

knockout of SPAK attenuates inflammation (LPS)-induced elevations in both CSF secretion and ventriculomegaly<sup>4</sup>. Accordingly, we also observed an elevation of p-SPAK signals in a PHH model (Fig. 5A, B). Notably, we observed an enrichment of p-SPAK in the ChP of  $A_{2A}R$ -OE mice (Fig. 5C, D). Subsequent Western blot analysis confirmed that the overexpression of  $A_{2A}R$  increased the levels of p-SPAK (Fig. 5E, F) in the ChP.

It has been reported that the phosphorylation of SPAK is facilitated through the PI3K-Akt pathway<sup>23</sup> and adenosine can engage the PI3K-PKA-mTOR cascade via interaction with  $A_{2A}R$ <sup>24,25</sup>. Thus, we postulated that  $A_{2A}R$  might regulate CSF secretion and ventricular size by augmenting the PI3K-PKA-dependent phosphorylation of SPAK. To test this hypothesis, we added either a selective PI3K inhibitor (GDC-0941) or a selective inhibitor of Akt (MK-2206) to mouse primary ChP epithelial cells that exhibited stable overexpression of  $A_{2A}R$ . After a 48-h interval, cells were collected for Western blot analysis, revealing a reduction in p-SPAK levels following either GDC-0941 or MK-2206 treatment (Fig. 5G–J).

Next, we designed an AAV2/5 vector carrying a shRNA targeting SPAK (AAV2/5-U6-shRNA (SPAK)-CMV-EGFP, SPAK-Kd) along with a control virus (AAV2/5-U6-scramble-CMV-EGFP, control). A virus combination (a mix of  $A_{2A}R$ -OE and SPAK-Kd virus) was subsequently injected into the lateral ventricle of WT mice (Fig. 5K). Mice injected with  $A_{2A}R$ -OE and AAV2/5-CMV-EGFP (control) virus were

used as the control group. Two weeks later, we conducted p-SPAK staining, which confirmed that the shRNA targeting SPAK effectively reduced the protein level of p-SPAK by 60% (Fig. 5L, M), with immunostaining of both HA ( $A_{2A}R$ ) and EGFP exclusively present in the ChP (Fig. 5N). The MRI analysis revealed that the suppression of p-SPAK in the ChP also mitigated the  $A_{2A}R$ -OE-induced ventriculomegaly (Fig. 5O–Q) and CSF hypersecretion (Fig. 5R, S). These findings further sustain that p-SPAK mediates the impact of  $A_{2A}R$  overexpression in excessive CSF secretion and enlarged brain ventricles.

### **$A_{2A}R$ control CSF secretion via NF- $\kappa$ B-mediated transcriptional control of $Na^+K^+$ -ATPase (ATP1A2)**

To further dissect the molecular mechanism underlying the  $A_{2A}R$ -mediated CSF secretion, we carried out a comparative RNA-seq analysis of ChP tissue harvested 14 days after ICV injections of either  $A_{2A}R$ -OE or control AAV into WT mice. We identified 67 differentially expressed genes (26 upregulated and 41 downregulated) in the  $A_{2A}R$ -OE group compared to the control group (Fig. 6A). The heatmap analysis of the top 50 genes visually illustrates significant alterations in transcript levels due to  $A_{2A}R$  overexpression (Fig. 6B). Gene ontology annotation revealed that the differentially expressed genes were predominantly enriched in ion transmembrane transporter activity, a process integral to CSF secretion (Fig. 6C). This substantiates the

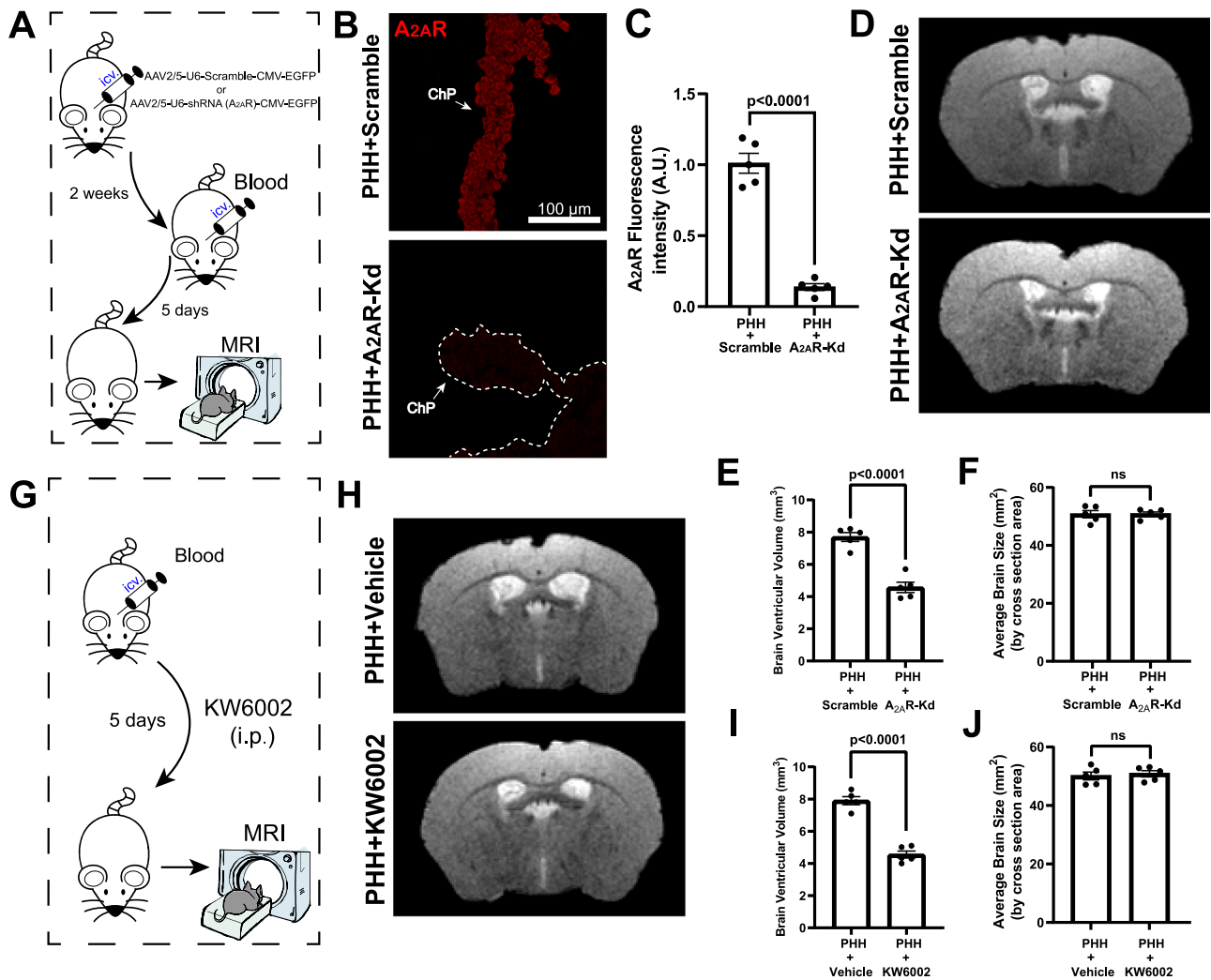


**Fig. 4 | Target inactivation of  $A_{2A}R$  in the choroid plexus (ChP) alleviates hydrocephalus pathology.** **A** Scheme of the experimental design to explore the role of  $A_{2A}R$  knockdown in the post-hemorrhagic hydrocephalus (PHH) model. **B** Representative immunofluorescence images of  $A_{2A}R$  in the ChP 5 days after ICV injection of autologous blood in mice previously treated with scramble (control) virus or virus expressing shRNA to down-regulate  $A_{2A}R$  ( $A_{2A}R$ -Kd). **C** Quantitative analysis of  $A_{2A}R$  fluorescence intensity showed in (B) ( $n = 5$ /group). **D** Representative fMRI images displaying brain ventricular size on day 5 after ICV injection of autologous blood in  $A_{2A}R$ -Kd and scramble (control) mice.

**E** Quantification of ventricle volumes as shown in (D) ( $n = 5$ /group). **F** Quantification of brain sizes as illustrated in (D) ( $n = 5$ /group). **G** Scheme of the experimental design to test the effect of the  $A_{2A}R$  antagonist (KW6002) in the PHH model. **H** Representative fMRI images showing brain ventricle dimensions on day 5 after ICV injection of autologous blood in mice treated with KW6002 or vehicle. **I** Quantification of ventricle volumes as depicted in (H) ( $n = 5$ /group). **J** Quantification of brain sizes as shown in (H) ( $n = 5$ /group). Unpaired two-tailed Student's  $t$  test. ns: non-significant. Data are mean  $\pm$  s.e.m. Source data are provided as a Source Data file.

involvement of aberrant  $A_{2A}R$  signaling in controlling CSF production in the ChP.

We further validated the RNA-seq data using qPCR. We selected certain candidate genes and found that the expression levels of *atp1a2* and *slc24a4* were reduced in the ChP of the  $A_{2A}R$ -OE group (Fig. 6D, E and S7). By contrast, overexpression of  $A_{2A}R$  did not alter the mRNA levels of *atp1a1*, *atp1b1*, and *atp1b2* (Fig. 6F–H). Since ATP1A2 belongs to the superfamily of  $Na^+$ - $K^+$ -ATPases and previous studies identified an ability of  $A_{2A}R$  to control  $Na^+$ - $K^+$ -ATPase activity in astrocytes<sup>18</sup>, we hypothesized that  $A_{2A}R$ -ATP1A2 signaling could be involved in the CSF secretion in the ChP. Indeed, we observed that the overexpression of  $A_{2A}R$  led to a decrease in the protein levels of ATP1A2 (Fig. 6I, J). Building upon our previous study, where we found that  $A_{2A}R$  signaling in ChP epithelium regulates the expression of CCL20 by activating the NF- $\kappa$ B pathway<sup>16</sup>, we hypothesized that  $A_{2A}R$  might control the expression of ATP1A2 via the NF- $\kappa$ B pathway. To test this, we tested the effect of an

inhibitor of NF- $\kappa$ B pathway transcriptional activity (JSH-23, 10  $\mu$ M) in a stable mouse primary ChP epithelial cells, which overexpressed  $A_{2A}R$ . After a 48-h treatment, cells were harvested for Western blot analysis. Strikingly, JSH-23 treatment markedly increased ATP1A2 protein levels (Fig. 6K, L). This strongly implies that  $A_{2A}R$  regulates the expression of ATP1A2 in a manner dependent on the NF- $\kappa$ B pathway.

Although it has been reported that the protein levels of  $Na^+$ - $K^+$ -ATPases are often decreased in models of hydrocephalus<sup>9</sup>, the precise role of  $Na^+$ - $K^+$ -ATPase subunits, including ATP1A2, remains unknown in hydrocephalus. Thus, we sought to address this gap of knowledge by overexpressing ATP1A2 in the ChP. This was achieved through an ICV injection into WT mice of AAV2/5 carrying cDNA of *atp1a2*, which was labeled with a His-tag at the C-terminal (Fig. 7A). The successful overexpression of ATP1A2 in the ChP was confirmed by mCherry/His-tag staining and Western blot analysis (Fig. 7B–D). In addition, we checked that overexpression of ATP1A2 in ChP tissue did not alter the

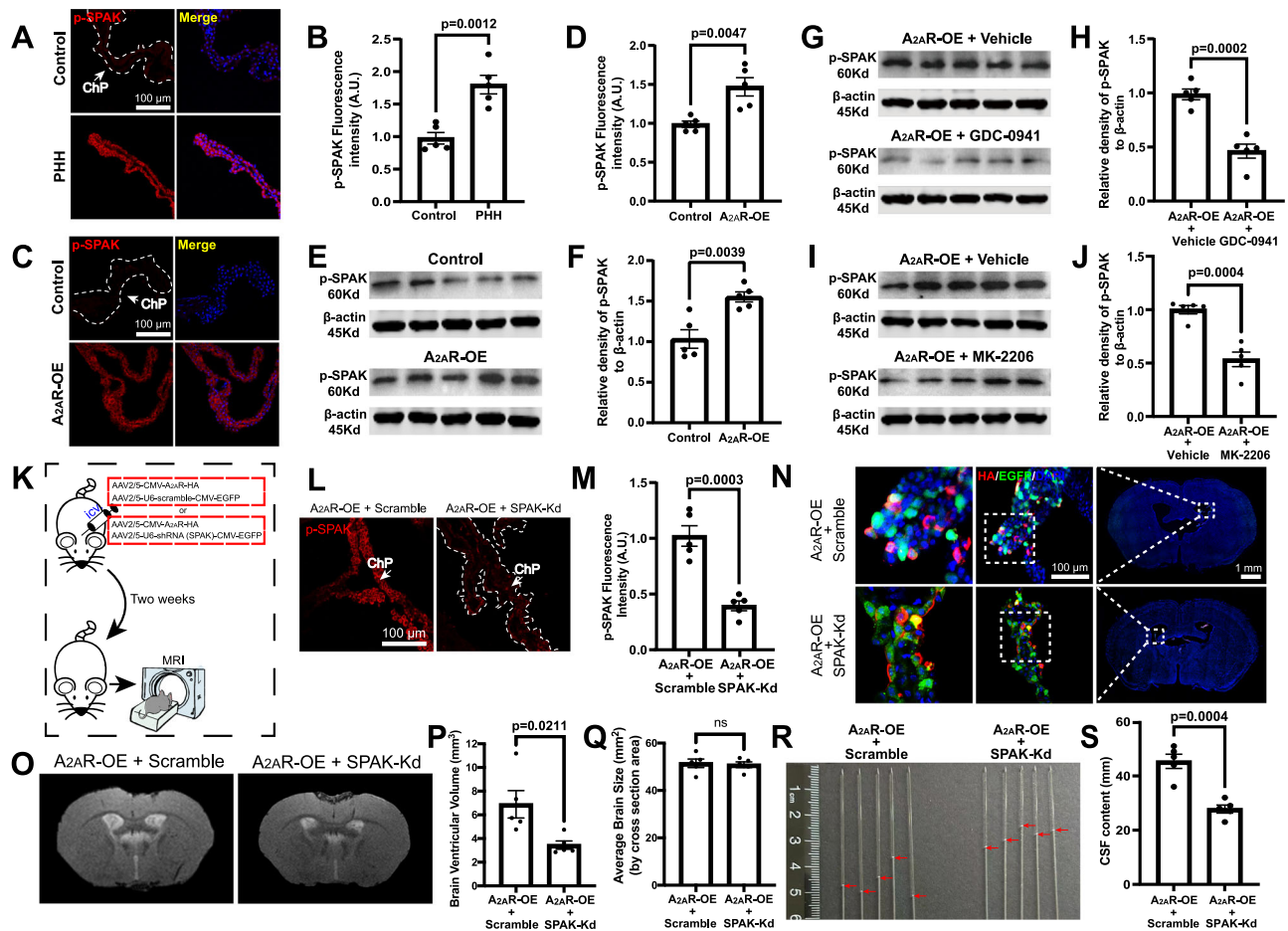


**Fig. 5 |  $A_{2A}R$  signaling controls cerebrospinal fluid (CSF) secretion via SPAK phosphorylation in the choroid plexus (ChP).** **A** Representative immunofluorescence images showing phosphorylated SPAK (p-SPAK) in the ChP of mice 5 days after the ICV injection of autologous blood. **B** Quantification of p-SPAK immunoreactivity in (A) ( $n = 5$ /group). **C** Representative immunofluorescence images depicting p-SPAK in the ChP of  $A_{2A}R$ -OE mice. **D** Quantification of p-SPAK immunoreactivity in (C) ( $n = 5$ /group). **E** Representative Western blots of p-SPAK in ChP lysates of mice 14 days after injection of AAV-control or AAV- $A_{2A}R$ -OE. **F** Quantification of p-SPAK protein levels in (E) ( $n = 5$ /group). **G** Representative immunoblots of p-SPAK in lysates of  $A_{2A}R$ -OE transfected primary ChP epithelial cells 48 h after treatment with the PI3K inhibitor GDC-0941 (0.5  $\mu$ M) or vehicle. **H** Quantification of p-SPAK protein levels in (G) ( $n = 5$ /group), showing that GDC-0941 prevented the increase of p-SPAK in  $A_{2A}R$ -OE transfected primary ChP epithelial cells. **I** Representative immunoblots of p-SPAK in lysates of  $A_{2A}R$ -OE transfected primary ChP epithelial cells 48 h after treatment with the Akt inhibitor MK-2206 (1  $\mu$ M) or vehicle. **J** Quantification of p-SPAK protein levels in (I) ( $n = 5$ /group).

showing that MK-2206 prevented the increase of p-SPAK in  $A_{2A}R$ -OE transfected primary ChP epithelial cells. **K** Scheme of the experimental design to investigate the impact on ventricular size of the downregulation of SPAK (SPAK-Kd) in mice overexpressing  $A_{2A}R$  in the ChP ( $A_{2A}R$ -OE). **L** Representative immunofluorescence images of p-SPAK in the ChP at day 14 after ICV-co-injection of  $A_{2A}R$ -OE and either scramble (control) or SPAK-Kd viruses. **M** Quantification of p-SPAK fluorescence intensity in (L) ( $n = 5$ /group). **N** Representative immunofluorescence images of HA-tag ( $A_{2A}R$ -OE) and EGFP (labeled with AAV-shRNA-SPAK or scramble) 14 days after in ICV-viral co-transfection ( $n = 5$ /group). **O** Representative fMRI images of brain ventricles obtained on day 14 following ICV co-injection of  $A_{2A}R$ -OE and either scramble (control) or SPAK-Kd viruses. **P** Quantification of ventricle volumes as shown in (O) ( $n = 5$ /group). **Q** Quantification of brain sizes as illustrated in (O) ( $n = 5$ /group). **R** Representative measurement of the CSF content of mice overexpressing  $A_{2A}R$  in the ChP with or without knockdown of SPAK. **S** Quantification of the CSF content in (R) ( $n = 5$ /group). Unpaired two-tailed Student's  $t$  test. ns: non-significant. Data are mean  $\pm$  s.e.m. Source data are provided as a Source Data file.

protein levels of  $A_{2A}R$  (Fig. 7E, F), which suggests that ATP1A2 may be a downstream gene of  $A_{2A}R$ .

Two weeks after the ICV injection of AAV2/5-CMV-ATP1A2-His (ATP1A2-OE) or AAV2/5-CMV-mCherry (control) into WT mice, MRI was used to quantify lateral ventricle volume. Strikingly, the overexpression of ATP1A2 in the ChP resulted in smaller ventricles in comparison to control mice (Fig. 7G, H). There were no discernible changes in the overall brain volume (Fig. 7I). In line with the reduced ventricular sizes, ATP1A2 overexpression in the ChP resulted in decreased CSF content (Fig. 7J, K).

Since the data suggest that  $A_{2A}R$  overexpression ( $A_{2A}R$ -OE) regulates CSF secretion by suppressing ATP1A2 expression, we next attempted a co-overexpression of  $A_{2A}R$  and ATP1A2 in the ChP to validate this proposed mechanism. This was achieved through the simultaneous ICV injection of  $A_{2A}R$ -OE and ATP1A2-OE viruses into

the lateral ventricle of WT mice (Fig. 7L). Mice receiving ICV injection of  $A_{2A}R$ -OE and AAV2/5-CMV-mCherry virus were considered as the control group. We observed that the HA signal ( $A_{2A}R$ ) and Histag signal (ATP1A2) were both selectively detected in the ChP (Fig. 7M). Two weeks after viral injection, MRI analysis revealed a reduction in ventricular size in mice with co-overexpression of  $A_{2A}R$  and ATP1A2, as compared to the control group (Fig. 7N–P). Similarly, the CSF volume in the co-overexpression group was lower than that in the controls (Fig. 7Q, R). These results demonstrate that overexpression of ATP1A2 can counteract the enlarged ventricle and excessive CSF secretion induced by overexpression of  $A_{2A}R$ . This might be relevant in hydrocephalus since we found that the protein level of ATP1A2 was partly restored after KW6002 treatment in the PHH model of hydrocephalus (Fig. S8).

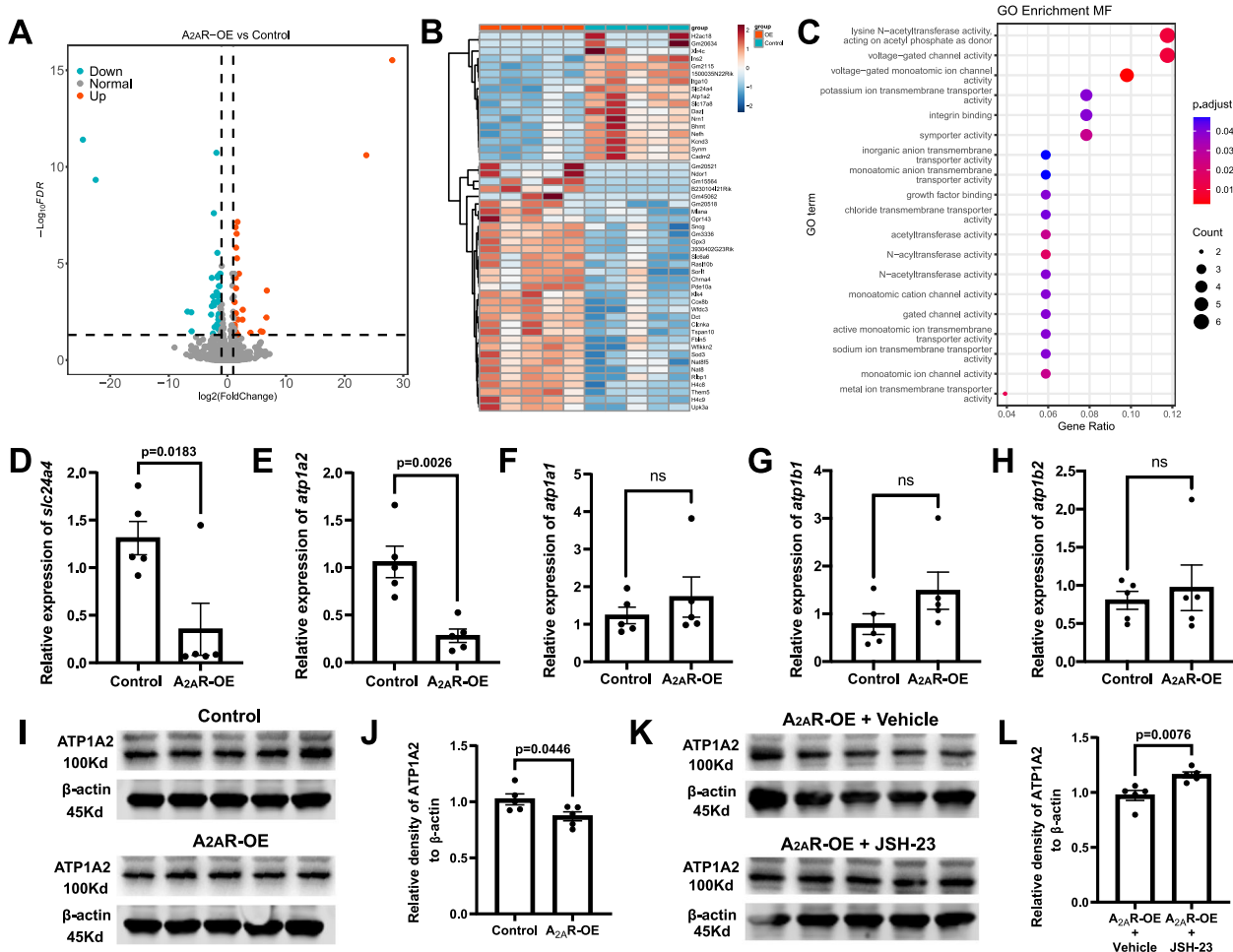


**Fig. 6 | Overexpression of A<sub>2A</sub>R modulates the expression of ion channel proteins in the choroid plexus (ChP).** A Volcano plot illustrating the differentially expressed genes (DEGs) identified upon A<sub>2A</sub>R overexpression (OE) in the ChP compared to the control group, based on bulk RNA-seq data ( $n = 5/\text{group}$ ). False Discovery Rate (FDR) was obtained by correcting the  $P$  value of the hypothesis testing results of DEGs using the Benjamin-Hochberg method. **B** Heatmap displaying the top 50 DEGs. **C** Gene ontology (GO) annotation of the DEGs observed in the bulk RNA-seq data. **D–H** Validation of the bulk RNA-seq data by qPCR analysis of candidate gene expression ( $n = 5/\text{group}$ ). **I** Representative immunoblots of ATP1A2

from ChP lysates of AAV-control vs. AAV-A<sub>2A</sub>R-OE mice (14 days after ICV-viral injection). **J** Quantitative analysis of ATP1A2 protein levels in **(I)** ( $n = 5/\text{group}$ ) shows that A<sub>2A</sub>R-OE in the ChP led to a reduction in ATP1A2 protein levels. **K** Representative immunoblots of ATP1A2 in lysates of A<sub>2A</sub>R-OE transfected primary ChP epithelial cells 48 h after treatment with the NF- $\kappa$ B inhibitor (JSH-23, 10  $\mu\text{M}$ ) or vehicle. **L** Quantification of ATP1A2 protein levels in **(K)** ( $n = 5/\text{group}$ ) showing that JSH-23 restored ATP1A2 levels in A<sub>2A</sub>R-OE transfected primary ChP epithelial cells. Unpaired two-tailed Student's  $t$  test. ns: non-significant. Data are mean  $\pm$  s.e.m. Source data are provided as a Source Data file.

### Elevated adenosine in ventricles directly triggers a hydrocephalus phenotype by activating A<sub>2A</sub>R signaling in the ChP

After unraveling the mechanism of A<sub>2A</sub>R-mediated control of CSF secretion, we next attempted to experimentally link the abnormal adenosine levels in the CSF of hydrocephalus patients with the A<sub>2A</sub>R-mediated CSF hypersecretion. To simulate the increased concentration of adenosine in hydrocephalus patients, we injected adenosine (or PBS as control) into the lateral ventricle of WT mice 4 times per day with an inter-injection interval of 6 h during 14 days, targeting a final concentration of 6  $\mu\text{M}$  (comparing to the basal concentration of adenosine at 2  $\mu\text{M}$  in normal mice, Fig. 1F) in a mouse CSF volume of 40  $\mu\text{L}$  (Fig. 8A). Of note, the chronic administration of adenosine upregulated the protein levels of A<sub>2A</sub>R in the ChP (Fig. 8B, C). The injected adenosine also promoted the phosphorylation of SPAK (Fig. 8D, E) and reduced the protein levels of ATP1A2 (Fig. 8F, G). Moreover, the chronic injection of adenosine resulted in enlarged ventricles (Fig. 8H, I) and CSF secretion (Fig. 8J, K). These data support the contention that elevated adenosine levels in the CSF may be a trigger of hydrocephalus. To grasp the source of adenosine, we tested the impact of impeding the extracellular formation of adenosine from

adenine nucleotides, which is mediated by CD73. We found that the selective knockdown of CD73 in ChP did not affect ventricle size (Fig. S9), which indicates that the burst of extracellular adenosine in the ChP controlling CSF secretion is unlikely to be derived from ATP release and catabolism.

Finally, we tested the impact of adenosine treatment during 14 days in mice that were first subject to a knockdown of A<sub>2A</sub>R selectively in the ChP (A<sub>2A</sub>R-Kd), as confirmed by the presence of EGFP signals restricted to the ChP (Fig. 8L). DAPI staining showed that the knockdown of A<sub>2A</sub>R in ChP prevented the phenotype of enlarged ventricles caused by adenosine (Fig. 8M, N). Conversely, we found that the injection of the selective A<sub>2A</sub>R agonist (CGS21680) induced CSF hypersecretion and enlarged ventricles (Fig. S10). This confirms our hypothesis that the elevated adenosine in the CSF triggered a hydrocephalus pathology by aberrant A<sub>2A</sub>R signaling in the ChP.

### Discussion

The present study establishes that elevated adenosine in the CSF and aberrant A<sub>2A</sub>R signaling in the ChP are key triggers of CSF hypersecretion and ventriculomegaly in hydrocephalus. This new adenosine

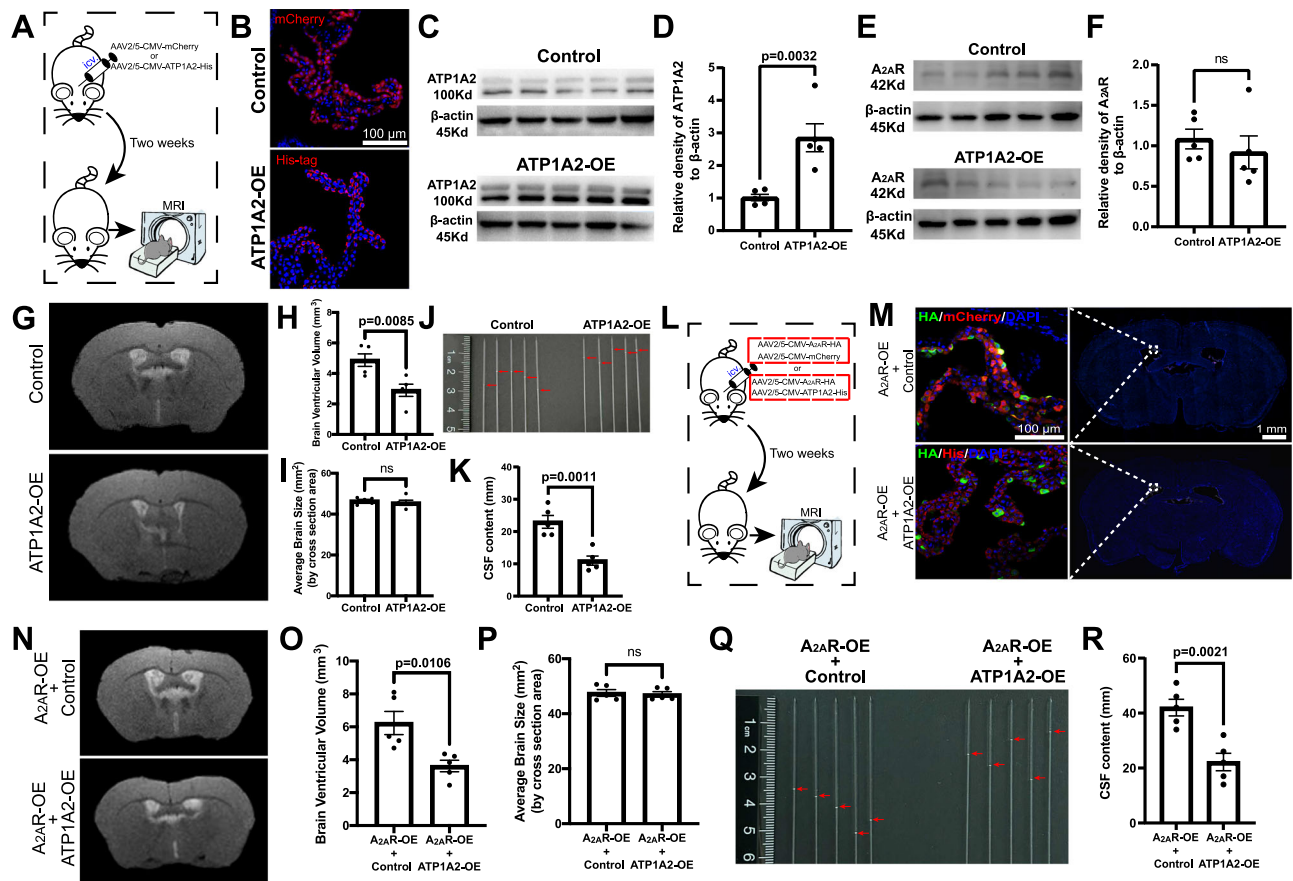


**Fig. 7 |  $A_2A_R$  signaling in the choroid plexus (ChP) controls cerebrospinal fluid (CSF) secretion through transcriptional regulation of ATP1A2.** **A** Scheme of the experimental design to investigate the impact of ATP1A2 overexpression in the ChP using fMRI. **B** Representative immunofluorescence images of His-tag (labeling ATP1A2) in the ChP infected with AAV2/5-ATP1A2-OE or control (AAV2/5-mCherry) virus 14 days after ICV viral injection ( $n = 5$ /group). **C** Representative immunoblots of ATP1A2 in ChP lysates from AAV-control vs. AAV-ATP1A2-OE mice (14 days after ICV-viral injection). **D** Quantification of ATP1A2 protein levels in (C) ( $n = 5$ /group). **E** Overexpression of ATP1A2 had no effect on  $A_2A_R$  density, as shown in the representative immunoblots of  $A_2A_R$  in ChP lysates from AAV-control vs. AAV-ATP1A2-OE mice (14 days after ICV-viral injection). **F** Quantification of  $A_2A_R$  protein levels in (E) ( $n = 5$ /group). **G** Representative fMRI images of brain ventricles day 14 after ATP1A2 overexpression in the ChP. **H** Quantification of ventricle volumes in control vs. ATP1A2-OE mice ( $n = 5$ /group). **I** Quantification of brain sizes in control

vs. ATP1A2-OE mice ( $n = 5$ /group). **J** Representative measurement of the CSF content in control vs. ATP1A2-OE group. **K** Quantification of the CSF content in (J) ( $n = 5$ /group). **L** Scheme of the experimental design detailing the co-overexpression of  $A_2A_R$  and ATP1A2. **M** Representative immunofluorescence images depicting HA-tag ( $A_2A_R$ ) and His-tag (ATP1A2) in brains co-transfected with  $A_2A_R$ -OE and either scramble (control) or ATP1A2-OE viruses that were collected 14 days after ICV viral co-injection ( $n = 5$ /group). **N** Representative fMRI images of brain ventricles obtained 14 days after ICV co-injection of  $A_2A_R$ -OE and either scramble (control) or ATP1A2-OE viruses. **O** Quantification of ventricle volumes in  $A_2A_R$ -OE without or with ATP1A2-OE in (N) ( $n = 5$ /group). **P** Quantification of brain sizes in  $A_2A_R$ -OE without or with ATP1A2-OE in (N) ( $n = 5$ /group). **Q** Representative measurement of the CSF content between  $A_2A_R$ -OE without or with ATP1A2-OE. **R** Quantification of CSF content in (Q) ( $n = 5$ /group). Unpaired two-tailed Student's *t* test. ns: non-significant. Data are mean  $\pm$  s.e.m. Source data are provided as a Source Data file.

hypothesis of the pathogenesis of hydrocephalus is based on the present observations that: (1) adenosine levels were increased in the CSF of patients with hydrocephalus and in mouse hydrocephalus model, which also displayed an increased  $A_2A_R$  density in the ChP; (2) the overexpression of  $A_2A_R$  selectively in the ChP was sufficient to induce a hydrocephalus-like phenotype, characterized by CSF hypersecretion and ventriculomegaly; (3) the targeted knockdown of  $A_2A_R$  in the ChP mitigated hydrocephalus; (4) likewise, the CSF hypersecretion and ventriculomegaly was ameliorated by systemic administration of the  $A_2A_R$  antagonist KW6002; (5)  $A_2A_R$  controlled the expression and density of active forms of proteins critical for CSF production in the ChP, namely phosphorylated SPAK and ATP1A2; (6) ventricular infusion of adenosine during 14 days triggered ChP- $A_2A_R$  upregulation, SPAK phosphorylation and ATP1A2 downregulation, leading to CSF hypersecretion and ventricle enlargement, an effect abolished by  $A_2A_R$  knockdown selectively in the ChP. Overall, this demonstrates that the aberrantly increased adenosine- $A_2A_R$  signaling within the CSF-ChP axis is a critical event in hydrocephalus pathology. This key role of aberrant CSF-adenosine and ChP- $A_2A_R$  in the control of CSF hypersecretion,

allows understanding the previously reported ability of caffeine (non-selective adenosine receptor antagonist) to improve developmental motor activities and reflexes in a mouse model of infant hydrocephalus<sup>26</sup> and the efficacy of diuretic, a sodium salicylate form of theobromine, which is equipotent to caffeine at adenosine receptors<sup>27</sup>, in 4 cases of pediatric hydrocephalus<sup>28</sup>. However, we are not aware of epidemiological studies linking caffeine consumption and hydrocephalus, which ought to be considered in the future.

The present identification that elevated CSF levels of adenosine and aberrant  $A_2A_R$  signaling in the ChP are key mediators of hydrocephalus also provides a straightforward rationale to understand how inflammation, hemorrhage, and stroke are major risk factors for the development of hydrocephalus<sup>1</sup>. RNA analysis of the CSF of patients with subarachnoid hemorrhage and post-hemorrhagic and autologous blood-induced post-hemorrhagic hydrocephalus identified immune cell infiltration, chemokine receptor signaling and secretory activity, and ligand-gated ion channel activity as the main molecular pathways<sup>29,30</sup>. Previous studies suggested that activation of Toll-like receptor 4 (TLR4) by proinflammatory cytokines and of the transient

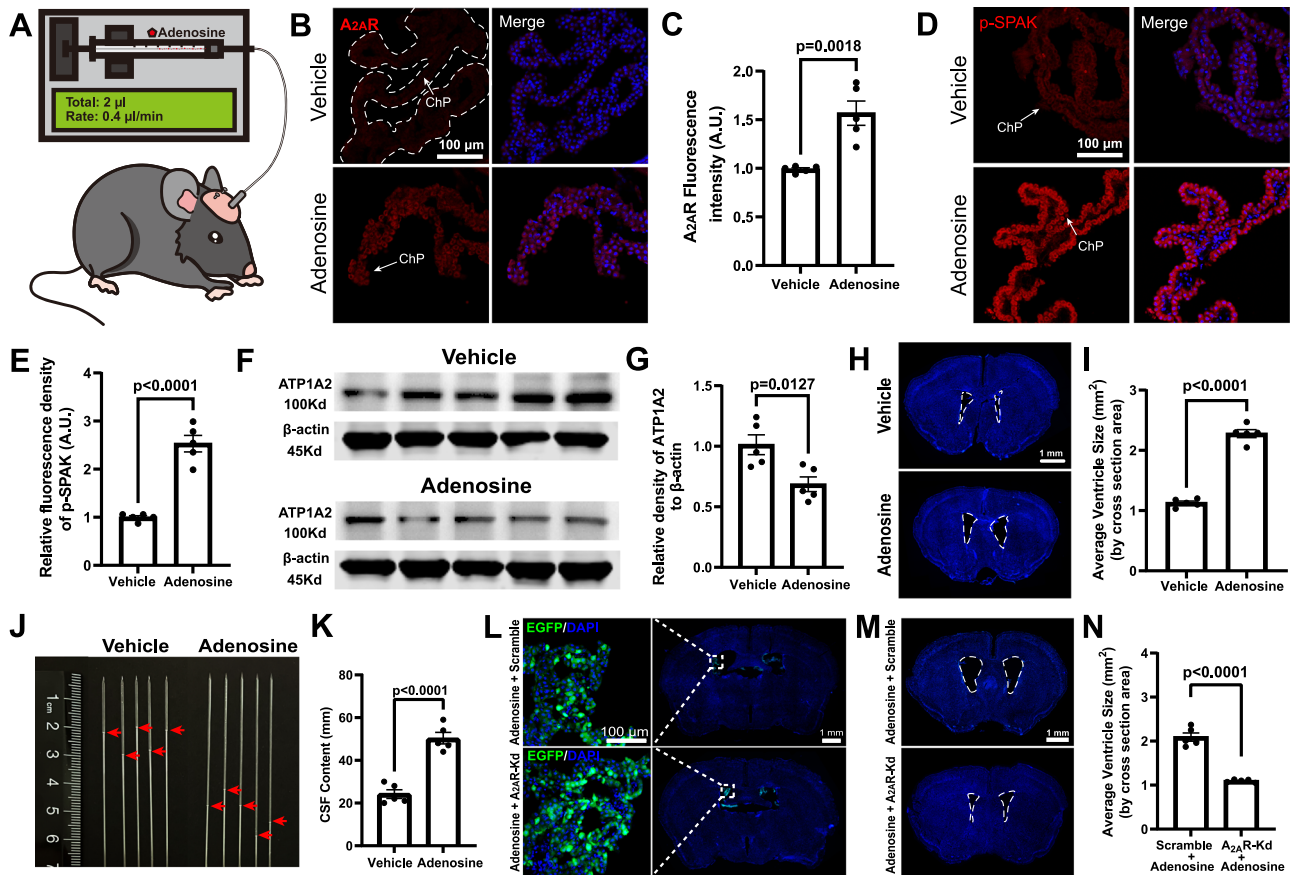


**Fig. 8 | ICV-injection of adenosine triggered a hydrocephalus phenotype via activation of A<sub>2A</sub>R signaling in the choroid plexus (ChP).** **A** Scheme of the experimental design to inject adenosine into the lateral ventricles of mice. **B** Representative images of A<sub>2A</sub>R immunostaining in the ChP of mice intermittently perfused with vehicle or adenosine for 14 days. **C** Quantification of A<sub>2A</sub>R fluorescence intensity in vehicle vs. adenosine ICV-perfused mice as illustrated in **(B)** ( $n = 5$ /group). **D** Representative images of p-SPAK immunostaining in the ChP of mice perfused ICV with vehicle or adenosine for 14 days. **E** Quantification of p-SPAK density in vehicle vs. adenosine ICV-perfused mice as illustrated in **(D)** ( $n = 5$ /group). **F** Representative immunoblots of ATP1A2 in ChP lysates from vehicle vs. adenosine ICV-perfused mice. **G** Quantification of ATP1A2 protein levels in **(F)** ( $n = 5$ /group), showed that ICV-exposure to adenosine led to a reduction in ATP1A2

levels after 14 days. **H** Representative DAPI-stained images showing that lateral ventricles were enlarged after 14 days of intermittent ICV-perfusion with adenosine. **I** Quantification of ventricular size as shown in **(H)** ( $n = 5$ /group). **J** Representative measurement of the CSF content of mice after 14 days of intermittent ICV-perfusion with adenosine or vehicle. **K** Quantification of CSF content in **(J)** ( $n = 5$ /group). **L** Representative immunofluorescence images of EGFP in brain sections transduced with AAV2/5-A<sub>2A</sub>R-Kd or control virus for 14 days and then ICV-perfused with adenosine for 14 days ( $n = 5$ /group). **M** Knockdown of A<sub>2A</sub>R in ChP reversed the enlarged brain ventricles induced by ICV-perfusion of adenosine ( $n = 5$ /group). **N** Quantification of ventricle areas in **(M)** ( $n = 5$ /group). Unpaired two-tailed Student's *t* test. Data are mean  $\pm$  s.e.m. Source data are provided as a Source Data file.

receptor potential vanilloid 4 (TRPV4) channel by the serum lipid lysophosphatidic acid could mediate CSF hypersecretion via the NKCC1<sup>4,9,30</sup>. In accordance with the involvement of inflammation as a trigger of hydrocephalus, early clinical trials showed that dexamethasone improved survival in young and adults suffering from tuberculous meningitis, presumably by reducing hydrocephalus and preventing infarction, based on the reduction of CSF hypersecretion and intra-cranial pressure<sup>31</sup>. Yet, blood or its component, hemin, does not activate the NKCC1 and NKA activity<sup>30</sup>, indicating that molecular signals, other than TLR4, may be responsible for sensing inflammatory/hemorrhage insults and activating NKCC1 and CSF hypersecretion. Adenosine emerges as a likely candidate to link not only inflammation but also other conditions, such as stroke or trauma, to the hypersecretion of CSF and hydrocephalus. In fact, adenosine levels are significantly augmented upon brain trauma or inflammation<sup>11–14</sup> since extracellular adenosine is an important intercellular signal, mediating adaptive responses to stressful conditions, such as upon trauma, infection or inflammation<sup>10</sup>. The CSF-hypersecretion and enlarged ventricle induced by autologous blood, overexpression of A<sub>2A</sub>R in ChP and kaolin all led to uniformly elevated adenosine levels in the ChP and CSF. This positions the increased adenosine levels as a

key signal to link noxious brain conditions with the flow and composition of the extracellular medium in the brain parenchyma by altering the production of CSF upon activation of A<sub>2A</sub>R in the ChP. This distinctive role of ChP-A<sub>2A</sub>R suggests that the A<sub>2A</sub>R is not a direct secretory protein like NKCC1, ATP1A2, and SPAK, which demonstrates a polarized localization in the ChP to control CSF production. Instead, we specifically demonstrate that ChP-A<sub>2A</sub>R is an indirect controller of CSF secretion through newly unveiled intracellular signaling mechanisms (PI3K/Akt and NF- $\kappa$ B) acting on targets with a polarized localization, namely SPAK and ATP1A2. Thus, A<sub>2A</sub>R is not required to display a polarized localization at the apical side of ChP to control CSF production. It should be noted that A<sub>2A</sub>R overactivation leading to hydrocephalus may be a maladaptive attempt to extreme a physiological process of adaptation of CSF flow to metabolic fluctuations of brain function, whereby adenosine generation is intrinsically associated with increased cellular metabolism<sup>32</sup> and the physiological activation of A<sub>2A</sub>R in the ChP provides a homeostatic increase of CSF production to reset the extracellular medium of the brain parenchyma. This physiological and homeostatic role of adenosine production and A<sub>2A</sub>R activation is in agreement with the presently observed decreased CSF production and reduced ventricular volumes upon ChP-specific

knockdown of A<sub>2A</sub>R and the previously reported ability of acutely administered caffeine (an adenosine receptor antagonist) to decrease CSF production<sup>33</sup> and intracranial pressure in control animals<sup>34</sup>. This homeostatic role is possibly driven by relatively small fluctuations of the extracellular levels of adenosine and by the low density of A<sub>2A</sub>R in the ChP in physiological conditions; in contrast, the large production of adenosine in conditions of inflammation, trauma or ischemic stroke<sup>11–14</sup> leads to an up-regulation of A<sub>2A</sub>R and the over-activation of this adenosine-A<sub>2A</sub>R signaling system becomes paramount in generating CSF hyperproduction leading to hydrocephalus. Interestingly, we now observed that the increase of extracellular adenosine triggers A<sub>2A</sub>R up-regulation as previously observed in models of Parkinson's disease<sup>35</sup>, which might be a general process involved in neurodegeneration whose mechanism remains unclear. Lastly, since adenosine generation is intrinsically associated with cellular metabolism and homeostasis<sup>32</sup>, the adenosine-mediated control of CSF secretion is expected to be ontogenically controlled in a homeostatic manner, providing new insights into the control of the CSF composition by development, metabolism, circadian rhythms, and hormones. An aspect that remains to be clarified is the source of the adenosine entraining the increased CSF accumulation and ventricular enlargement. Since inflammation, a known trigger of hydrocephalus, involves a robust release of ATP<sup>36</sup>, one hypothesis would be that ATP-derived adenosine might be the source of the observed A<sub>2A</sub>R overactivation leading to hydrocephalus. The lack of the effect of ChP knockdown of CD73 on ventricle size indicates that the surge of extracellular adenosine in the ChP in PHH is unlikely derived from extracellular conversion of ATP into adenosine. An alternative is that the burst of extracellular adenosine controlling CSF secretion might be derived from a direct outflow of adenosine through equilibrated nucleoside transporters from the cells in the ChP. However, both the cellular sources and the mechanism of increased adenosine levels in the ChP leading to hydrocephalus remains to be investigated.

This study also advances prospects of hydrocephalus therapy by identifying aberrant A<sub>2A</sub>R signaling as the key trigger of two parallel molecular and signaling mechanisms: (1) a control of the phosphorylation of the SPAK through the recruitment of PI3K-Akt, as previously demonstrated in other cell types, namely in endothelial cells<sup>37</sup>; (2) a modification of gene expression, namely of ATP1A2, through the control of NF- $\kappa$ B, as previously shown in other cell types<sup>38</sup>. We now show that there is a simultaneous need of altering the efficiency of ionic transmembrane flow through the SPAK as well as a decreased energy-driven exchange of cations through ATP1A2 in the ChP to sustain an increased CSF production: in fact, the pharmacological or genetic correction of each of the two pathways operated by aberrant A<sub>2A</sub>R signaling is sufficient to prevent the condition of hydrocephalus triggered by A<sub>2A</sub>R overexpression. Our current data converge with previous RNA-seq analyses pinpointing ligand-gated ion channel activity as the final common pathway for CSF hypersecretion in hydrocephalus; our findings fully align with previous reports of an increased SPAK phosphorylation and decreased protein levels of Na<sup>+</sup>-K<sup>+</sup>-ATPase or decreased phosphorylated Na<sup>+</sup>-K<sup>+</sup>-ATPase in rats with post-hemorrhagic or post-ischemic hydrocephalus<sup>9</sup> and also with the postulated role of TLR4-NF- $\kappa$ B signaling and of SPAK kinase in coupling the immune response in the ChP through its interactions with cytokine receptors and ion transport proteins<sup>4,39</sup>. A major advance provided by the present study was the identification of the causal role selectively of ATP1A2 in the development of hydrocephalus, rather than other Na<sup>+</sup>-K<sup>+</sup>-ATPase isoforms<sup>40</sup>, all identified in the brush border membrane of the ChP<sup>41</sup> and with different sensitivities to ouabain. This selective A<sub>2A</sub>R-ATP1A2 interaction is reminiscent of our previous demonstration that A<sub>2A</sub>R signaling in astrocytes regulates glutamate uptake via the regulation of ATP1A2 activity<sup>18</sup>. Thus, our finding that ChP-A<sub>2A</sub>R controls ATP1A2 prompts the new and exciting possibility of managing hydrocephalus by indirectly and selectively controlling of

ATP1A2 amongst the different Na<sup>+</sup>-K<sup>+</sup>-ATPase isoforms with different pharmacological properties and functional efficiencies<sup>42</sup>. Although we demonstrated that A<sub>2A</sub>R-mediated changes in molecular signals (p-SPAK and ATP1A2) underlying hydrocephalus, our limited current knowledge of the mechanisms underlying hydrocephalus makes it possible that maybe there might exist are other pathways involved in hydrocephalus in parallel with A<sub>2A</sub>R signals. This makes the robust size effect of A<sub>2A</sub>R surprising in view of the numerous pathways converging on the control of CSF dynamics and ventricle size. Although we have now provided detailed support for the involvement of an A<sub>2A</sub>R-SPAK/ATP1A2 pathway, it is possible that other pathways may be simultaneously affected by A<sub>2A</sub>R, such as *slc24a4* or *slc17a8* and eventually aquaporins. Importantly, some of these pathways may be controlled at the protein rather than at the transcriptomic level as identified for aquaporin-4<sup>43</sup>, and future work should be aimed at detailing the likely multiple pathways affected by A<sub>2A</sub>R to understand its striking and robust effect of ventricle volume. This effect of A<sub>2A</sub>R on ventricle size was not previously noted, probably because the impact of A<sub>2A</sub>R blockade in the ChP to decrease ventricle size was larger in physiological conditions than in the models of hydrocephalus, the same occurring in TBI<sup>3</sup> and EAE models<sup>16</sup>.

Our present proposal of the adenosine hypothesis of hydrocephalus prompts the tempting contention that pharmacologically targeting aberrant A<sub>2A</sub>R signaling in ChP may be a novel and superior therapeutic strategy with high translational potential for controlling hydrocephalus. Thus, the systemic administration of NKCC1 inhibitors may preferentially interfere with NKCC1 either peripherally or within the brain vasculature, likely plaguing the efficacy and patient tolerability of NKCC1 inhibitors (such as acetazolamide and furosemide) for hydrocephalus treatment. Indeed, hemorrhage-induced CSF hypersecretion and hydrocephalus are sensitive to intrathecal delivery, but not to systemic exposure, of the SPAK-NKCC1 inhibitor, bumetanide<sup>9</sup>. In this regard, ChP-A<sub>2A</sub>R signaling may represent the most promising target for the treatment of hydrocephalus, in view of the localized aberrant increase of adenosine in the CSF of patients with hydrocephalus, in line with the elevated levels of inosine, an adenosine metabolite, in the CSF of infants with hydrocephalus<sup>44</sup>. Notably, we demonstrated that the systemic administration of KW6002 ameliorated the hydrocephalus phenotypes. This is of particular relevance since there is a dire need for effective pharmacotherapy for hydrocephalus, and repurposing the FDA-approved A<sub>2A</sub>R antagonist, KW6002<sup>45</sup>, emerges as a new therapeutic option to manage hydrocephalus. Conversely, the benefit of KW6002 in Parkinson's disease could be dampened by its reduction of CSF dynamics, reducing glymphatic activity and aggregate clearance to bolster PD pathology. This might be counteracted by the parallel effect of KW6002 in the ChP to increase the tightness of the ChP barrier, as shown in a EAE model<sup>16,46</sup>, reducing immune cell infiltration and dampening PD pathology. Careful monitoring of the impact of KW6002 on PD disease progression, considering its multiple actions on the ChP, including CSF production and increased integrity of the ChP tight junctions, are warranted to clarify the exact overall effect.

## Methods

### Study approval

All experiments adhered to the guidelines outlined in the US National Institutes of Health Guide for the Care and Use of Laboratory Animals. The animal experiments were approved by the Animal Experimentation Regulation of Wenzhou Medical University (xmsq2021-0012). Additionally, the collection of CSF samples from patients was approved by the Human Ethics Committee of Ningbo University (KY2023SL185-01). Written informed consent was obtained from all human participants for the use of their samples and data in research. However, specific consent for the publication of potentially identifiable information was not obtained. Therefore, to protect participant

privacy, all individual data (such as exact age and the hospital name) have been presented in an aggregated form (age data are presented as mean  $\pm$  SD) to ensure that no individual participant can be identified.

### Human subjects

Human CSF samples were collected with written informed consent from the department of Neurology and Neurosurgery at a single tertiary medical center in Ningbo, China, following ethical approval (KY2023SL185-01). To prevent potential adenosine degradation, the collected human CSF samples were rapidly frozen in liquid nitrogen and subsequently stored at  $-80^{\circ}\text{C}$ . The remaining samples were stored at  $-80^{\circ}\text{C}$ . Due to the small volume of the CSF samples, they are generally not shared.

### Quantification of adenosine levels in human CSF using ultra-high performance liquid chromatography (UPLC)

To construct the adenosine standard curve, we initially dissolved adenosine powder (Sigma, A9251-25G) into the mobile phase (50 mmol/L  $\text{NaH}_2\text{PO}_4$  and methanol in a volume ratio of 7:3) to obtain a series of adenosine solutions with varying concentrations between 0.0625 and 5  $\mu\text{mol/L}$ . We measured the absorbance of these standard samples at 254 nm using a UPLC instrument (Thermo, Accela 1250). The mobile phase flowed at a rate of 400  $\mu\text{L/min}$ , while the column temperature was maintained at  $30^{\circ}\text{C}$ . Ultimately, we generated a linear standard curve ( $R^2 > 0.999$ ).

A double-blind method was used to assess adenosine concentrations in the collected human CSF samples. Following the collation of case data and the assignment of sample numbers, the CSF samples were transferred to the tester. After a preliminary evaluation of all patient CSF samples, the tester divided them into high and low-concentration groups. For the high-concentration group, 20  $\mu\text{L}$  of 0.025% dipyrindamole (Sigma, D9766-1G) and 800  $\mu\text{L}$  of iced methanol were added to 200  $\mu\text{L}$  of CSF samples, which were then placed on ice for 15 min. The samples then underwent centrifugation at  $15,294 \times g$  for 15 min at  $4^{\circ}\text{C}$  to remove any debris and were filtered through 0.22  $\mu\text{m}$  sterile polyether sulfone membranes. The samples were dried using nitrogen gas, and the resulting powder was reconstituted in 400  $\mu\text{L}$  of mobile phase (diluted 2 $\times$ ). For the low-concentration group, 60  $\mu\text{L}$  of 0.025% dipyrindamole and 2400  $\mu\text{L}$  of iced methanol were added to 600  $\mu\text{L}$  of CSF samples, which were also kept on ice for 15 min. These samples were subjected to the same centrifugation and filtration processes as above. After drying, the powder was redissolved in 300  $\mu\text{L}$  of mobile phase (concentrated 2 $\times$ ). Then, the absorbance of these processed samples was measured after UPLC separation and the data were analyzed using MATLAB software.

### Animals

Wild-type (WT) C57BL/6 mice (male and female), aged 6–8 weeks and weighing 22–25 g, were purchased from SPF Biotechnology Co., Ltd. (Beijing, China). The mice were housed in an environment maintained at  $25^{\circ}\text{C}$  with a standard 12-h light and 12-h dark cycle and were provided with ad libitum access to both food and water.

### Isolation of the ChP

The mice were subjected to deep anesthesia using 1% sodium pentobarbital and subsequently perfused with pre-cooled PBS. The entire brain was then carefully extracted and quickly placed on an ice slab. Under a microscope, the ChP was quickly dissected from the lateral, third, and fourth ventricles and then transferred into 1.5 mL tubes. These samples were rapidly frozen using liquid nitrogen and stored in a  $-80^{\circ}\text{C}$  for subsequent experimental procedures.

### Immunofluorescence

The coronal brain sections (20  $\mu\text{m}$  thick) were initially rinsed three times with PBS, followed by permeabilization in a solution containing

PBS with 0.3% Triton X-100 (Roche Diagnostics GmbH, 11332481001), 1% bovine serum albumin (BSA, from Amresco, 0332-100G) and 5% normal donkey serum (Jackson, 017-000-121) at room temperature for 2 h. Next, the sections were incubated overnight at  $4^{\circ}\text{C}$  with the following primary antibodies against: A<sub>2A</sub>R (Frontier Institute, A2A-Go-Af700, 1:200), p-SPAK (Millipore, 07-2273, 1:300), IBA-1 (Wako, 019-19741, 1:400), CD31 (Bio-technique, AF3628, 1:200), ICAM-1 (Abcam, ab179707, 1:400), MHC-II (Invitrogen, 2028-06-19, 1:200), HA-tag (Cell Signaling Technology, #3724, 1:200), ATP1A2 (Proteintech, 16836-1-AP, 1:200), and 488-conjugated His-tag (Proteintech, CL488-66005, 1:100). The sections then underwent three PBS wash cycles before incubation with secondary antibodies coupled to either Alexa Fluor 594 or 555, for 2 h at room temperature (except for the His-tag mAb). Fluorescence images were acquired using a confocal microscope (LSM900, Zeiss), and subsequent analysis of fluorescence intensity was performed with the ImageJ software.

### Quantitative real-time PCR (qPCR)

RNA was extracted using the Trizol reagent, and cDNA was synthesized with the cDNA synthesis kit (Vazyme, R323-01). PCR amplification was carried out employing the SYBR Green kit (Takara, RR82LR). The expression levels were normalized to the reference gene (*ppia*) using the  $2^{-\Delta\Delta C_t}$  method. The primer sequences were displayed in Table S2.

### Western blotting

ChP tissues or cells were lysed using RIPA buffer supplemented with protease inhibitors (Bimake, B14001) and a phosphatase inhibitor cocktail (Bimake, B15001). After homogenization, the samples were centrifuged at  $10,621 \times g$  for 10 min to remove cellular debris. Protein concentration was measured using the BCA assay kit (Beyotime, P0010). The samples were denatured in 5 $\times$  sodium dodecyl-sulfate (Beyotime, P0015) by heating at  $90^{\circ}\text{C}$  for 8 min. Equal amounts of proteins were loaded and separated by electrophoresis on either a 10% gradient polyacrylamide gel (Vazyme, E303-01) or an 8% gradient polyacrylamide gel (Vazyme, E302-01). The gel was then transferred onto a 0.45  $\mu\text{m}$  PVDF membrane (GE Amersham, 10600023) at 300 mA for 1–2 h in ice water. The membrane was then blocked with Tris buffered saline with 0.1% Tween 20 (TBST) and 1% BSA (BBI, A600332-0100) and incubated overnight at  $4^{\circ}\text{C}$  with primary antibodies against:  $\beta$ -actin (Proteintech, 66009-1-Ig, 1:2000), A<sub>2A</sub>R (A2A-Go-Af700, Frontier Institute, 1:200), p-SPAK (Millipore, 07-2273, 1:1000) or ATP1A2 (Invitrogen, PA5-101902, 1:600). Finally, the membrane was incubated with horseradish peroxidase-conjugated secondary antibodies for 90 min at room temperature. The membrane was visualized using a molecular imager (Bio-Rad, ChemiDoc XRS+).

### Targeted knockdown or overexpression of genes in the ChP

Mice were anesthetized using 1% pentobarbital sodium, and their top fur was trimmed. Erythromycin eye ointment was applied to prevent light-induced damage. Subsequently, the mice were immobilized in a stereotaxic apparatus, and 2  $\mu\text{L}$  of various AAV2/5 constructs were separately injected into the lateral ventricles at the following coordinates: AP:  $-0.58$ ; ML:  $-1.10$ ; DL:  $-2.20$ . The injection rate was set at 400 nL/min, and the needle remained in place for an additional 20 min before withdrawal. The AAV2/5 constructs used were as follows: AAV2/5-U6-shRNA (A<sub>2A</sub>R)-CMV-EGFP ( $6.27 \times 10^{12}$  vg/mL), AAV2/5-U6-scramble-CMV-EGFP ( $6.21 \times 10^{12}$  vg/mL), AAV2/5-CMV-A<sub>2A</sub>R-HA ( $5.19 \times 10^{12}$  vg/mL), AAV2/5-CMV-EGFP ( $5.54 \times 10^{12}$  vg/mL), AAV2/5-U6-shRNA (SPAK)-CMV-EGFP ( $5.22 \times 10^{12}$  vg/mL), AAV2/5-CMV-ATP1A2-His ( $5.77 \times 10^{12}$  vg/mL) and AAV2/5-CMV-mCherry ( $5.80 \times 10^{12}$  vg/mL). For the co-expression of two viruses in the ChP, a mixture of 4  $\mu\text{L}$  of various viruses was injected into the lateral ventricles at the coordinates mentioned above. The combinations of different viruses administered simultaneously were as follows: AAV2/5-CMV-A<sub>2A</sub>R-HA and AAV2/5-U6-shRNA (SPAK)-CMV-EGFP, AAV2/5-CMV-A<sub>2A</sub>R-HA and AAV2/5-U6-scramble-CMV-EGFP, AAV2/5-CMV-

A<sub>2A</sub>R-HA and AAV2/5-CMV-ATPIA2-His, AAV2/5-CMV-A<sub>2A</sub>R-HA and AAV2/5-CMV-mCherry. The volume ratio of the two viruses in each mixture was 1:1. All mice were allowed a two-week recovery period after viral injection before subsequent experiments.

### Model of post-hemorrhagic hydrocephalus (PHH)

The PHH model was performed as previously described<sup>47,48</sup>. In brief, 20  $\mu$ L of autologous blood or sterile PBS were administered into the right lateral ventricle (AP: -0.58; ML: +1.10; DL: -2.20) at a rate of 5  $\mu$ L/min. Then, the needle was left in place for 10 min and carefully removed at a rate of 1 mm/min. The incision in the skin was then sealed using medical glue (Vetbond, 3M 1469sb), and the mice were placed on a warm heating pad for recovery.

### Model of obstructive hydrocephalus

The mice were anesthetized with 1% pentobarbital sodium. Subsequently, a 3  $\mu$ L injection of either 20% kaolin (Sigma-Aldrich, 1332-58-7) or sterile PBS was administered into the right lateral ventricle (AP: -0.58; ML: +1.10; DL: -2.20) at a rate of 500 nL/min, and the needle was left in place for 7 min before being carefully withdrawn. The incision in the skin was then sealed using medical glue, and the mice were placed on a warm heating pad for the recovery period.

### ICV injection of Evans blue dye

Briefly, 3  $\mu$ L of Evans blue dye (0.5%, Sigma-Aldrich, E2125) were injected into the right lateral ventricle (AP: -0.58; ML: +1.10; DL: -2.20) using a steady rate of 400 nL/min, keeping the Hamilton syringe in place for 30 min before withdrawal. The mice were then placed on a warm heating pad for an additional hour to ensure adequate circulation of the dye within the CSF spaces. Mice were then transcardially perfused, and their brains were harvested and sagittally cut. Images were then captured to assess the patency of CSF circulation.

### CSF collection and measurement

CSF was collected from the anesthetized mice by inserting a glass capillary into the cisterna magna and allowing it to sit for 15 min. The length of the glass capillary filled with CSF was promptly measured using a ruler.

### Drug administration

KW6002 (Sundia MediTech Company Ltd), a selective A<sub>2A</sub>R antagonist, was dissolved in a 1:1 premixture of dimethyl sulfoxide (DMSO) (Sigma-Aldrich, 276855) and corn oil (Thermo Scientific, 8001-30-7). This mixture was further diluted in saline (in a 3:7 volume ratio) to achieve complete dissolution of the KW6002 suspension. Three days after the ICV injection of kaolin, the mice received daily intraperitoneal injections of either the vehicle or KW6002 (5 mg/kg).

### Primary culture of ChP epithelial cells

The ChP cell cultures were produced as described in our previous study<sup>16</sup>. Briefly, following a perfusion with PBS, the ChPs were dissected, digested with trypsin (0.25%) for 20 min and dissociated by pipetting. The cells were cultured in L-polylysine-coated 24-well plates for 5 days in Dulbecco's modified Eagle's medium (DMEM)/Ham's F12 medium supplemented with 10% fetal bovine serum, 1 mM L-glutamine, 1 mM sodium pyruvate, penicillin/streptomycin (100 U/mL), insulin (5 ng/mL), 20  $\mu$ M arabinosylcytosine, sodium selenite (5 ng/mL) and epidermal growth factor (10 ng/mL).

### Over-expression of A<sub>2A</sub>R in the primary ChP epithelial cells

In brief, the primary ChP epithelial cells were transfected with the constructed lentivirus (CMV-A<sub>2A</sub>R-3Flag-Ubi-ZsGreen-IRES-Puromycin). After 48 h, the cells were screened with puromycin (1  $\mu$ g/mL, 2.5  $\mu$ g/mL). The ZsGreen-positive cells were then used for follow-up assays.

### Effects of PI3K/Akt or NF- $\kappa$ B inhibitors

In brief, the primary ChP epithelial cells, stably transfected to over-express A<sub>2A</sub>R, were treated with either JSH-23 (10  $\mu$ M, a NF- $\kappa$ B transcriptional activity inhibitor, Sigma-Aldrich, 749886-87-1), MK-2206 (1  $\mu$ M, a selective Akt inhibitor, MedChemExpress, HY-108232), GDC-0941 (0.5  $\mu$ M, a selective PI3K inhibitor, MedChemExpress, HY-50094) or vehicle. After 48 h, the cells were collected for Western blot analysis.

### Whole-genome RNA sequencing (RNA-seq)

Illumina library construction adhered to the manufacturer's instructions (Illumina, USA) at ApexBio Technology LLC (Shanghai, China). Subsequently, reads were aligned to the mouse genome (mm10) using STAR version 2.5. The aligned reads were quantified using the Homer software (analyze repeats). Differentially expressed genes were identified by DESeq2<sup>49</sup> with five replications for each sample. A cut-off criterion of  $|\log_2|\text{fold-change}|>1.2$  with a  $P < 0.05$  was applied. The false discovery rate was obtained by correcting the  $P$  value of the hypothesis testing results of differentially expressed genes using the Benjamin Hochberg method. To analyze gene ontology and KEGG pathway categories, ClusterProfiler<sup>50</sup> was employed.

### ICV-infusion of adenosine

A dosing administration device (Kedou Brain-Computer Technology) was implanted into the right lateral ventricle and immobilized on the surface of mouse skull by the instant adhesive gel. One week later, adenosine solution (80  $\mu$ M) was prepared with 0.5% methyl cellulose (Sigma-Aldrich, M0512-100G) and filtered through the 0.22  $\mu$ m sterile PES membrane (JETBIOFIL, 230701-052-A). CGS21680 (80  $\mu$ M, ab12053) was prepared with dimethyl sulfoxide (Beyotime, AT038-500ml) and filtered through the 0.22  $\mu$ m sterile PES membrane. Adenosine or CGS21680 was immediately infused into the mouse lateral ventricle via the implanted cannula (Kedou Brain-Computer Technology) connected to the immobilized skull device by the syringe pump (R462, RWD) at the rate of 0.4  $\mu$ L/min for 5 min. A similar infusion was performed 4 times a day for 2 weeks.

### Magnetic resonance imaging (MRI)

Mice were subjected to imaging using a small animal MRI system (Bruker BioSpec 94/20 USR, 9.4 T) after being anesthetized with isoflurane. To maintain body temperature, a warm pad was utilized. All axial images were obtained under the following conditions: TE/TR = 33/2500; Ave = 4; RARE = 8; slice thickness = 0.3 mm. Brain sizes and ventricle volumes were calculated through manual segmentation with the assistance of ImageJ or 3Dslicer software. It is worth noting that ventricle areas were not excluded during the measurement of brain sizes.

### Statistical analysis

All statistical analyses were performed with GraphPad Prism 9.0. The data are screened for normality using the Kolmogorov-Smirnov test and are presented as mean  $\pm$  s.e.m. Two-tailed Mann-Whitney U test was used to compare the data of adenosine levels in hydrocephalus patients and controls, as the data sets did not follow normal distribution (the data are presented as median and interquartile range). Two-tailed Student's  $t$  test was used in other data. No adjustments for multiple comparisons were applied in the initial analysis.

### Reporting summary

Further information on research design is available in the Nature Portfolio Reporting Summary linked to this article.

### Data availability

RNA-seq datasets were deposited into BioProject database under number PRJNA1353615. All sequencing data is publicly available. Source data are provided with this paper.

## References

1. Bramall, A. N., Anton, E. S., Kahle, K. T. & Fecci, P. E. Navigating the ventricles: novel insights into the pathogenesis of hydrocephalus. *EBioMedicine* **78**, 103931 (2022).
2. Saunders, N. R., Dziegielewska, K. M., Fame, R. M., Lehtinen, M. K. & Liddelow, S. A. The choroid plexus: a missing link in our understanding of brain development and function. *Physiol. Rev.* **103**, 919–956 (2023).
3. Zhang, Z. et al. NLRP3 inflammasome-mediated choroid plexus hypersecretion contributes to hydrocephalus after intraventricular hemorrhage via phosphorylated NKCC1 channels. *J. Neuroinflammation* **19**, 163 (2022).
4. Robert, S. M. et al. The choroid plexus links innate immunity to CSF dysregulation in hydrocephalus. *Cell* **186**, 764–785.e721 (2023).
5. Karimy, J. K. et al. Inflammation in acquired hydrocephalus: pathogenic mechanisms and therapeutic targets. *Nat. Rev. Neurol.* **16**, 285–296 (2020).
6. Bothwell, S. W., Janigro, D. & Patabendige, A. Cerebrospinal fluid dynamics and intracranial pressure elevation in neurological diseases. *Fluids Barriers CNS* **16**, 9 (2019).
7. Steffensen, A. B. et al. Cotransporter-mediated water transport underlying cerebrospinal fluid formation. *Nat. Commun.* **9**, 2167 (2018).
8. Xu, H. et al. Choroid plexus NKCC1 mediates cerebrospinal fluid clearance during mouse early postnatal development. *Nat. Commun.* **12**, 447 (2021).
9. Karimy, J. K. et al. Inflammation-dependent cerebrospinal fluid hypersecretion by the choroid plexus epithelium in posthemorrhagic hydrocephalus. *Nat. Med.* **23**, 997–1003 (2017).
10. Chen, J. F., Eltzschig, H. K. & Fredholm, B. B. Adenosine receptors as drug targets—what are the challenges? *Nat. Rev. Drug Discov.* **12**, 265–286 (2013).
11. Park, T. S., Van Wylen, D. G., Rubio, R. & Berne, R. M. Increased brain interstitial fluid adenosine concentration during hypoxia in newborn piglet. *J. Cereb. Blood Flow. Metab.* **7**, 178–183 (1987).
12. Phillis, J. W., Walter, G. A. & Simpson, R. E. Brain adenosine and transmitter amino acid release from the ischemic rat cerebral cortex: effects of the adenosine deaminase inhibitor deoxycoformycin. *J. Neurochem.* **56**, 644–650 (1991).
13. Headrick, J. P., Bendall, M. R., Faden, A. I. & Vink, R. Dissociation of adenosine levels from bioenergetic state in experimental brain trauma: potential role in secondary injury. *J. Cereb. Blood Flow. Metab.* **14**, 853–861 (1994).
14. Yoshida, Y. et al. Adenosine and neopterin levels in cerebrospinal fluid of patients with neurological disorders. *Intern. Med.* **38**, 133–139 (1999).
15. Cunha, R. A. How does adenosine control neuronal dysfunction and neurodegeneration? *J. Neurochem.* **139**, 1019–1055 (2016).
16. Zheng, W. et al. Choroid plexus-selective inactivation of adenosine A(2A) receptors protects against T cell infiltration and experimental autoimmune encephalomyelitis. *J. Neuroinflammation* **19**, 52 (2022).
17. Mills, J. H., Alabanza, L. M., Mahamed, D. A. & Bynoe, M. S. Extracellular adenosine signaling induces CX3CL1 expression in the brain to promote experimental autoimmune encephalomyelitis. *J. Neuroinflammation* **9**, 193 (2012).
18. Matos, M., Augusto, E., Agostinho, P., Cunha, R. A. & Chen, J. F. Antagonistic interaction between adenosine A2A receptors and Na<sup>+</sup>/K<sup>+</sup>-ATPase- $\alpha$ 2 controlling glutamate uptake in astrocytes. *J. Neurosci.* **33**, 18492–18502 (2013).
19. Brown, P. D., Davies, S. L., Speake, T. & Millar, I. D. Molecular mechanisms of cerebrospinal fluid production. *Neuroscience* **129**, 957–970 (2004).
20. Sitkovsky, M. V. et al. Physiological control of immune response and inflammatory tissue damage by hypoxia-inducible factors and adenosine A2A receptors. *Annu. Rev. Immunol.* **22**, 657–682 (2004).
21. Bucheimer, R. E. & Linden, J. Purinergic regulation of epithelial transport. *J. Physiol.* **555**, 311–321 (2004).
22. Ye, M. et al. Adenosine A(2A) receptor controls the gateway of the choroid plexus. *Purinergic Signal.* **19**, 135–144 (2023).
23. Nishida, H. et al. Phosphatidylinositol 3-kinase/Akt signaling pathway activates the WNK-OSR1/SPAK-NCC phosphorylation cascade in hyperinsulinemic db/db mice. *Hypertension* **60**, 981–990 (2012).
24. Shi, L. et al. Adenosine interaction with adenosine receptor A2a promotes gastric cancer metastasis by enhancing PI3K-AKT-mTOR signaling. *Mol. Biol. Cell* **30**, 2527–2534 (2019).
25. Mori, Y., Higuchi, M., Masuyama, N. & Gotoh, Y. Adenosine A2A receptor facilitates calcium-dependent protein secretion through the activation of protein kinase A and phosphatidylinositol-3 kinase in PC12 cells. *Cell Struct. Funct.* **29**, 101–110 (2004).
26. Olopade, F., Femi-Akinlosotu, O., Ibitoye, C. & Shokunbi, T. Probing caffeine administration as a medical management for hydrocephalus: an experimental study. *Pediatr. Neurol.* **135**, 12–21 (2022).
27. Valada, P., Alçada-Morais, S., Cunha, R. A. & Lopes, J. P. Thebromine targets adenosine receptors to control hippocampal neuronal function and damage. *Int. J. Mol. Sci.* **23**, 10510 (2022).
28. PETERMAN, M. G. THE KETOGENIC DIET IN THE TREATMENT OF EPILEPSY: A PRELIMINARY REPORT. *Am. J. Dis. Child.* **28**, 28–33 (1924).
29. Lolansen, S. D. et al. Inflammatory markers in cerebrospinal fluid from patients with hydrocephalus: a systematic literature review. *Dis. Markers* **2021**, 8834822 (2021).
30. Lolansen, S. D. et al. Posthemorrhagic hydrocephalus associates with elevated inflammation and CSF hypersecretion via activation of choroidal transporters. *Fluids Barriers CNS* **19**, 62 (2022).
31. Thwaites, G. E. et al. Dexamethasone for the treatment of tuberculous meningitis in adolescents and adults. *N. Engl. J. Med.* **351**, 1741–1751 (2004).
32. Cunha, R. A. Adenosine as a neuromodulator and as a homeostatic regulator in the nervous system: different roles, different sources and different receptors. *Neurochem. Int.* **38**, 107–125 (2001).
33. Han, M. E. et al. Regulation of cerebrospinal fluid production by caffeine consumption. *BMC Neurosci.* **10**, 110 (2009).
34. Israelsen, I. M. E., Westgate, C. S. J., Kamp-Jensen, C., Jensen, R. H. & Eftekhari, S. Effects of caffeine on intracranial pressure and pain perception in freely moving rats. *Headache* **63**, 1220–1231 (2023).
35. Meng, F. et al. CD73-derived adenosine controls inflammation and neurodegeneration by modulating dopamine signalling. *Brain* **142**, 700–718 (2019).
36. Di Virgilio, F., Vultaggio-Poma, V., Falzoni, S. & Giuliani, A. L. Extracellular ATP: a powerful inflammatory mediator in the central nervous system. *Neuropharmacology* **224**, 109333 (2023).
37. Ahmad, A., Schaack, J. B., White, C. W. & Ahmad, S. Adenosine A2A receptor-dependent proliferation of pulmonary endothelial cells is mediated through calcium mobilization, PI3-kinase and ERK1/2 pathways. *Biochem. Biophys. Res. Commun.* **434**, 566–571 (2013).
38. Kermanian, F., Soleimani, M., Ebrahimzadeh, A., Haghiri, H. & Mehdizadeh, M. Effects of adenosine A2a receptor agonist and antagonist on hippocampal nuclear factor-kB expression preceded by MDMA toxicity. *Metab. Brain Dis.* **28**, 45–52 (2013).
39. Yan, Y. & Merlin, D. Ste20-related proline/alanine-rich kinase: a novel regulator of intestinal inflammation. *World J. Gastroenterol.* **14**, 6115–6121 (2008).
40. Blanco, G. & Mercer, R. W. Isozymes of the Na-K-ATPase: heterogeneity in structure, diversity in function. *Am. J. Physiol.* **275**, F633–F650 (1998).

41. Baasch Christensen, I. et al. Multiple Na, K-ATPase subunits colocalize in the brush border of mouse choroid plexus epithelial cells. *Int. J. Mol. Sci.* **22**, 1569 (2021).
42. Krivoš, I. I. [Regulatory function of the Na,K-ATPase alpha2 isoform]. *Biofizika* **57**, 771–788 (2012).
43. Dias, L. et al. Impact of glucocorticoid-associated stress-like conditions on aquaporin-4 in cultured astrocytes and its modulation by adenosine A(2A) receptors. *J. Neurochem.* **169**, e16299 (2025).
44. Schmidt, H., Siems, W. G., Grune, T. & Grauel, E. L. Concentration of purine compounds in the cerebrospinal fluid of infants suffering from sepsis, convulsions and hydrocephalus. *J. Perinat. Med.* **23**, 167–174 (1995).
45. Chen, J. F. & Cunha, R. A. The belated US FDA approval of the adenosine A(2A) receptor antagonist istradefylline for treatment of Parkinson's disease. *Purinergic Signal.* **16**, 167–174 (2020).
46. Qi, C. et al. Adenosine A(2A) receptor-mediated interactions between Th1(+) T cells and the choroid plexus epithelium via IFN-gamma signalling control T-Cell infiltration in experimental autoimmune encephalomyelitis. *Cell Commun. Signal* **23**, 94 (2025).
47. Zhu, W. et al. Changes in motor function, cognition, and emotion-related behavior after right hemispheric intracerebral hemorrhage in various brain regions of mouse. *Brain Behav. Immun.* **69**, 568–581 (2018).
48. Shen, D. et al. Ferroptosis in oligodendrocyte progenitor cells mediates white matter injury after hemorrhagic stroke. *Cell Death Dis.* **13**, 259 (2022).
49. Love, M. I., Huber, W. & Anders, S. Moderated estimation of fold change and dispersion for RNA-seq data with DESeq2. *Genome Biol.* **15**, 550 (2014).
50. Wu, T. et al. clusterProfiler 4.0: a universal enrichment tool for interpreting omics data. *Innovation* **2**, 100141 (2021).

## Acknowledgements

This research received financial support from the following sources: the Research Fund for International Senior Scientists (Grant No. 82150710558 to J.F.C.), the National Natural Science Foundation of China (Grant No. 31800903 to W.Z.), the Zhejiang Provincial Natural Science Foundation of China (Grant No. LMS25H090008 to W.Z.), the Science & Technology Initiative ST12030-Major Projects (Grant No. 2021ZD0203400 to J.F.C.), the Department of Science and Technology of Zhejiang Province (Grant No. 2023ZY1011 to W.Z.), the Ningbo Major Research and Development Plan Program (Grant No. 2023Z196 to W.Z.), the Ningbo Medical Science and Technology Project (Grant No. 2023Y03 to Z.Y.L.) and the Ningbo Medical and Health Leading Academic Discipline Project (Grant No. 2022-F04 to H.C.W.).

## Author contributions

W.Z. and J.F.C. designed and conceived the research; W.Z., L.X.H., Y.W.Y., X.H.L., W.C.C. and Y.W.J. prepared the tables and figures; W.Z., L.X.H., Y.W.Y., X.H.L., J.W., W.C.C., Y.W.J., Y.H.C. and C.Z. performed the experiments and analysis; Z.Y.L., H.C.W., Y.J.W., S.W.L. and K.F. collected the CSF from hydrocephalus patients and controls. W.Z., R.A.C. and J.F.C. wrote and revised the manuscript.

## Competing interests

The authors declare no competing interests.

## Additional information

**Supplementary information** The online version contains supplementary material available at <https://doi.org/10.1038/s41467-025-66776-8>.

**Correspondence** and requests for materials should be addressed to Wu Zheng, Zhongyue Lv or Jiang-Fan Chen.

**Peer review information** *Nature Communications* thanks Miriam Echevarria and the other anonymous reviewer(s) for their contribution to the peer review of this work. A peer review file is available.

**Reprints and permissions information** is available at <http://www.nature.com/reprints>

**Publisher's note** Springer Nature remains neutral with regard to jurisdictional claims in published maps and institutional affiliations.

**Open Access** This article is licensed under a Creative Commons Attribution-NonCommercial-NoDerivatives 4.0 International License, which permits any non-commercial use, sharing, distribution and reproduction in any medium or format, as long as you give appropriate credit to the original author(s) and the source, provide a link to the Creative Commons licence, and indicate if you modified the licensed material. You do not have permission under this licence to share adapted material derived from this article or parts of it. The images or other third party material in this article are included in the article's Creative Commons licence, unless indicated otherwise in a credit line to the material. If material is not included in the article's Creative Commons licence and your intended use is not permitted by statutory regulation or exceeds the permitted use, you will need to obtain permission directly from the copyright holder. To view a copy of this licence, visit <http://creativecommons.org/licenses/by-nc-nd/4.0/>.

© The Author(s) 2025